Running head: Spatiotemporal mapping of legume root exudation

***Address correspondence for this author:**
Philip S. Poole
Department of Plant Sciences, University of Oxford
South Parks Road, OX1 3RB Oxford, United Kingdom
Telephone: +44 - (0)1865 - 275023
E-mail: philip.poole@plants.ac.ox.uk

Research area: Breakthrough technologies

Title: Lux bacterial biosensors for *in vivo* spatiotemporal mapping of root secretion

Francesco Pini[a], Alison K. East[a,b], Corinne Appia-Ayme[b], Jakub Tomek[c], Ramakrishnan Karunakaran[b], Marcela Mendoza-Suárez[a,b], Anne Edwards[b], Jason J. Terpolilli[b], Joshua Roworth[a], J. Allan Downie[b] and Philip S. Poole[a,b*]

[a] Department of Plant Sciences, University of Oxford, South Parks Road, Oxford OX1 3RB, UK

[b] Department of Molecular Microbiology, John Innes Centre, Norwich Research Park, Norwich NR4 7UH, UK

[c] Department of Physiology, Anatomy and Genetics, University of Oxford, Sherrington Road, Oxford OX1 3PT, UK

One sentence summary:

Development of a suite of rhizobial *lux* reporters to map *in vivo* root exudation, spatially and temporally.

Author Contributions

Conceived and designed the experiments: FP, AKE, and PSP. Performed the experiments: FP, RK, MMS, CAA, AKE, JJT, JR, and AE. Analyzed the data: FP, AKE, and PSP. Software development: JT. Wrote the paper: FP, AKE, JAD, and PSP.

Footnotes:

Financial source: This work was funded by the Biotechnology and Biological Sciences Research Council [grant numbers BB/K001868/1, BB/K001868/2] and a BBSRC Institute Strategic Programme Grant (BIO) at the John Innes Centre.

Address correspondence to philip.poole@plants.ac.ox.uk

The author responsible for distribution of materials integral to the findings presented in this article in accordance with policy described in the Instructions for Authors (www.plantphysiol.org) is:

Philip S. Poole (philip.poole@plants.ac.ox.uk)

Manuscript information:

Word and character count: 219 words in abstract, and 10,069 words in text, comprising Introduction and References

Abstract

Plants engineer the rhizosphere to their advantage by secreting various nutrients and secondary metabolites. Coupling transcriptomic and metabolomic analysis of the *Pisum sativum* rhizosphere, a suite of bioreporters has been developed in *Rhizobium leguminosarum* bv. *viciae* 3841, and these detect metabolites secreted by roots in space and time. Fourteen bacterial *lux*-fusion bioreporters, specific for sugars, polyols, amino acids, organic acids or flavonoids, have been validated *in vitro* and *in vivo*. Using different bacterial mutants (*nodC, nifH*), the process of colonization and symbiosis has been analyzed, revealing compounds important in the different steps of the rhizobial-legume association.

Dicarboxylates and sucrose are the main carbon sources within the nodules; in ineffective (*nifH)* nodules, particularly low levels of sucrose were observed suggesting that plant sanctions affect carbon supply to nodules. In contrast, high *myo*-inositol levels were observed prior to nodule formation and also in *nifH* senescent nodules. Amino-acid biosensors showed different patterns: a GABA biosensor was active only inside nodules, whereas the phenylalanine bioreporter showed a high signal also in the rhizosphere. The bioreporters were further validated in vetch, producing similar results. In addition, vetch exhibited a local increase of *nod*-gene inducing flavonoids at sites where nodules subsequently developed. These bioreporters will be particularly helpful to understand the dynamics of root exudation and the role of different molecules secreted into the rhizosphere.

Additional keywords: Biosensor, Rhizosphere, Root secretion, Legume nodulation, *Pisum, Vicia,* Exudate

Introduction

Due to root secretion, the narrow zone surrounding roots known as the rhizosphere, is a nutrient-rich region where plants encounter a diversity of microbes, fungi, invertebrates and the roots of other plants (Turner et al., 2013a). The constant improvement of sequencing techniques has rapidly increased acquisition of knowledge about rhizosphere communities (Turner et al., 2013b). It is now evident that there is a two-way dialogue, with plants actively shaping their rhizosphere community; this in turn, profoundly alters plant growth e.g. by improving plant nutrient uptake (Philippot et al., 2013). Secretion patterns from roots differ between plants (Biedrzycki and Bais, 2009) and despite much research on the role of chemical signals in mediating belowground interactions (Huang et al., 2014), many factors have not yet been identified (Badri et al., 2009). In addition, spatial and temporal variations in root secretions have never been clearly elucidated. Plant roots secrete large amounts of different compounds into the soil and about 20% of photosynthate is released through the roots (Kaiser et al., 2015). As a consequence of this, compared to bulk soil, the rhizosphere is a rich source of compounds sustaining bacterial growth. This results in the attraction to the rhizosphere of many different microorganisms, amongst them both pathogens and plant growth-promoting bacteria (Huang et al., 2014). Different techniques have been used to study this complex environment; e.g. proteomics, metabolomics and transcriptomics, (reviewed by: Sørensen et al., 2009; Oburger and Schmidt, 2016), but the results obtained with many of these different methodologies is that they give only a single 'snapshot' as it has not been possible to follow the same plant during the course of its development. Current 2D and 3D non-invasive imaging techniques to examine the physical architecture of the plant roots using radiation-based techniques of X-ray microfocus-computed tomography or synchrotron tomography have been described (Mooney et al., 2011). These techniques are powerful at revealing root architecture and development but do not yield information about chemical secretion by roots.

In response to plant secretions, bacteria modify expression of specific genes based on the molecules present in the rhizosphere (Ramachandran et al., 2011). Linking this with a method to monitor gene expression, we have used bacteria as biosensors to detect where and when specific molecules are secreted by plant roots. Bioluminescence is non-invasive and allows measurement of *in situ* differences in the secretion of specific

compounds in a semi-quantitative way. Lux biosensors have already been successfully used (Darwent et al., 2003), but lack of a simple system for image acquisition and complex experimental settings have so far limited routine use. Improvement of the technologies available and an increased knowledge of the bacterial transcriptomic response to roots, now gives us the chance to develop a suite of biosensors. These biosensors have been constructed using *Rhizobium leguminosarum* biovar *viciae*. Rhizobia are alpha-proteobacteria, ubiquitous within soil and able to establish nitrogen-fixing symbioses with specific legumes. Perception of environmental signals plays a pivotal role in association between plants and bacteria (Pini et al., 2011) and *R. leguminosarum* biovar *viciae* modifies its transcriptomic profile in different rhizospheres (Ramachandran et al., 2011). Moreover, the association of *R. leguminosarum* biovar *viciae* with peas has been studied in depth (Oldroyd et al., 2011; Terpolilli et al., 2012; Udvardi and Poole, 2013), making *R. leguminosarum* biovar *viciae* one of the best candidates for biosensor development to investigate the rhizosphere. Pea and vetch plants have been used allowing us to monitor both the rhizosphere and the process of nodulation. Applications of this methodology will be multiple and are not restricted to leguminous plants; e.g. screening plant mutant libraries for those altered in secretion from roots or observing different exudations during seed germination.

RESULTS

Solute Specificity of Biosensors

To spatially and temporally investigate secretion in the rhizosphere, we need biosensors able to detect compounds exuded into this environment. The idea that effective biosensors could be constructed using the control elements for expression of specific bacterial genes, often encoding components of solute transporters or enzymes with precise substrate recognition, has been previously described (Tecon and van der Meer, 2006; Yagi, 2007; Sørensen et al., 2009). Induction of expression of genes encoding transporters in the presence of their transported solute led to the identification of the substrates of many ATP-binding cassette (ABC) and tripartite ATP-independent periplasmic (TRAP) transporter systems of *Sinorhizobium meliloti* (Mauchline et al., 2006). Building on these data, Ramachandran *et al*. (Ramachandran et al., 2011) determined which genes of *R. leguminosarum* biovar *viciae* strain 3841 (Rlv3841) are differentially expressed in the rhizospheres of pea, alfalfa and sugar beet, leading to identification of metabolites inducing expression of genes encoding both transport systems and metabolic enzymes. As many of these genes were induced in the rhizosphere in response to specific solutes, we sought to use their expression profiles to develop a suite of biosensors. These biosensors can be grouped by classification of inducer: i) sugars and polyols, ii) organic acids, iii) amino acids and iv) flavonoids (Table I). How each biosensor was selected is described below.

Eleven genes whose expression was induced in the rhizosphere during plant colonization by Rlv3841 of the pea rhizosphere (Ramachandran et al., 2011) were selected for biosensor development (Table I). These include seven solute-specific transport systems (which may transport plant-derived compounds, or those from any source e.g. fungi, other bacteria, within the rhizosphere), and four enzymes from metabolic pathways that are up-regulated during rhizosphere colonization (Table I). To increase the suite of biosensors, an additional two genes were included on the basis of microarray data that show differential expression in response to pea root exudate (Table I) (Ramachandran et al. 2011). The fourteenth biosensor is based on a salicylic acid-inducible export system for salicylic acid (Tett et al., 2014), which is known to be an important signaling molecule in plant defense. Whilst an inducer of gene expression was already known for many of these, the only previous characterization of pRL90085, RL4218, and pRL120556 was that their expression was induced either in the

rhizosphere or by pea-root exudate (Table II).

To develop the *lux*-based induction biosensors, the promoter regions upstream of the selected genes were used, often including the whole coding sequence of any upstream regulatory gene. Following PCR amplification, each region was cloned into the luminescence vector (pIJ11268, a plasmid stably inherited in rhizobia), in front of the bacterial *luxCDABE* operon (Frederix et al., 2014) (Supplemental Table S1). As these biosensors are plasmid-based it is possible to transfer them into different bacterial backgrounds, e.g. mutant strains of *R. leguminosarum* or other species of bacteria, although their expression in heterologous hosts may be limited by regulatory elements (Galardini et al., 2015). Each of the fourteen *lux* reporters was tested on 26 different sugars and polyols and/or on a set of 18 selected compounds (organic acids, amino acids and plant metabolites) to establish the specificity of induction of *lux* expression from each of the bioreporters (Table I, Supplemental Table S2). Nine of the biosensors were induced by only a single compound tested: i.e. the polyols erythritol (pRL90085) and *myo*-inositol (RL4655; *intA*); the organic acids formate (RL4393; *fdsG*), malonate (RL0992; *matA*), tartrate (RL0996) and salicylic acid (RL1329; *salA* encoding an export system for salicylic acid induced by the presence of this molecule (Tett et al., 2014)); the amino acids phenylalanine (RL1860; *phhA*) and GABA (RL0102; *gabT*); and the flavonoid hesperetin (pRL100185; *nodABC*) (Table I). These solutes are considered to be specific inducers, i.e. the specific luminescence is ≥10-fold the specific luminescence induced by the other solutes tested (apart from bioreporters for erythritol, formate, and GABA which have relatively high expression in the presence of a variety of chemically unrelated substrates (background), but show ≥4-fold the specific luminescence of other solutes). However, this definition of specificity, in no way excludes the possibility that these bioreporters may also react with other compounds similar to the molecules which elicit the primary response, but not tested in this work, e.g. it is known that *nod* genes are induced by a variety of different flavonoids (Maj et al., 2010; Maxwell et al., 1989). Another two sugar biosensors were induced by two closely related compounds tested (Table I): i) by two aldopentoses, xylose or lyxose (RL2720; *rbsC*) or ii) induction by the di-saccharide sucrose was also achieved by the tri-saccharide raffinose (pRL120556), presumably because either the biosensor recognizes the sucrose 1-2 β linkage in the di-/tri-saccharide or raffinose is metabolized to sucrose. A further two bioreporters were induced by three closely related compounds; i) the C4-dicarboxylic

organic acids succinate, malate and aspartate all cause induction of a single biosensor (RL3424; *dctA*) and ii) the polyol mannitol (C6) is the main inducer in biosensor (RL4218) although, a weaker induction is elicited also by its isomer sorbitol, and C5 adonitol (Table I) Sorbitol and adonitol are not considered specific inducers as their specific luminescence is <40% that of mannitol (Table I). One bioreporter was induced by six of the tested sugars and polyols, with the main inducer being the mono-saccharide fructose (RL0489; *frcB*). Induction was also seen with di-saccharides lactulose (4-O-β-D-galactopyranosyl-β-D-fructofuranose) and sucrose (α -D-glucopyranosyl-(1$\rightarrow$2)- β -D-fructofuranoside). These sugars all share a common structure containing a molecule of β-D-fructofuranose. Furthermore, this biosensor was induced by the polyols mannitol and sorbitol and the monosaccharide mannose. In this case, it is likely that induction occurs due to the catabolism of these compounds to fructose. The fourteen biosensors were used in the following experiments and are henceforth referred to by the compound that elicits the highest-fold change in *lux* expression (Table I). Provided rhizobial survival is not affected, these biosensors should be able to detect the presence of the compound/s for which they are specific, not only in the rhizosphere, whether they are derived from plants, from other bacteria or another source, but also in many other environments.

To discover the limits of detection for each biosensor, the sensitivity (the minimum concentration which causes induction) of the main inducer was determined using a range of different solute concentrations. The sensitivity ranges from the ability to detect levels of 1 μM for mannitol and hesperetin to 10 mM for formate and malonate (Table I).

Data Extraction from Images using NightCROP

Plants were analyzed using the NightOWL, a molecular imaging system linked to a sensitive charged-coupled device (CCD) camera, which allows measurement of light output from the Lux proteins. Images collected were first analyzed with the IndiGO software but although it was used to obtain data for nodules and vetch plants (output in cps / mm^2), a limitation of this software is that it is unable to do an automatic segmentation of the picture, so NightCROP, a custom MATLAB script, was developed. The script uses the SeNeCA algorithm (Tomek et al., 2013) to segment roots from the background in the light intensity channel, discarding those segments smaller than 1000

pixels. The information on the position of the roots is then used on the luminescence channel to specifically detect the fluorescence signal coming from the roots (Supplemental Fig. S1).

In vivo Mapping of Bacterial Colonization of Pea Roots

Before using the suite of bioreporters to map the rhizosphere, we examined colonization by *R. leguminosarum* bv *viciae* of pea roots *in planta* using Lux mapping. Rlv3841 containing pIJ11282, expressing Lux constitutively under the control of the *nptII* promoter (Frederix et al., 2014), was used to inoculate pea seedling roots and the luminescent images revealed the location on the root of metabolically active Rlv3841. Lux expression relies on the bacteria having enough energy in the form of ATP to drive this energetically expensive production of light. Pea roots were imaged every 3-4 days until 22 dpi, with nodules becoming visible to the naked eye at 11-15 dpi.

At 4 and 8 dpi, luminescence from Rlv3841 colonization was mainly detected in the elongation zone of the lateral and primary roots (Fig. 1). At 11 dpi, overall luminescence was reduced probably due to energy depletion of the bacteria, (Fig. 1), although a signal was still detectable at a lower level (Supplemental Fig. S2). After 15 dpi, there was an increase of the signal concurrent with nodule development, and luminescence was then stable in nodules until 18 dpi, decreasing at 22 dpi, probably due to a general decline of plant health under these growth conditions. This constitutive Lux fusion is an energy sensor that is very effective at showing initial colonization and the total energy available to the bacteria, but must be used with caution in longer-term imaging, dues to depletion of bacterial energy reserves resulting in loss of signal.

In vivo Mapping of Metabolites on Pea Roots and in Nodules

The composition of pea root exudate was determined by metabolomic analysis of hydroponically-grown plants. Although plants grown in different conditions may differ in the composition of their root exudates, metabolomic analysis of these exudates is able to give important indications on compounds that it may be possible to retrieve from the rhizosphere. With the exception of formate, salicylic acid, and hesperetin, the targets of our biosensors were among the 376 compounds detected in exudate from 23 d-old peas (Table II, Supplemental Table S3). A microarray experiment comparing Rlv3841 grown with and without addition of the same 23 d-old pea root exudates used for the metabolomic analysis was also performed. Results from this are compared to a

290 microarray where *R. leguminosarum* was inoculated into the pea rhizosphere and then
291 harvested 1 dpi from 21 d-old plants (Ramachandran et al., 2011) (Table II). Of the
292 fourteen genes used to develop biosensors, eleven (all except those detecting malonate,
293 salicylic acid and GABA) showed increased (> 3-fold) expression with added pea root
294 exudate and/or in pea rhizosphere-grown cells (Ramachandran et al., 2011) (Table II),
295 however, relative increases in expression in these two experiments do not correlate
296 particularly well. This discrepancy is likely to be due to differences in concentrations
297 of solutes in the two experiments. Indeed, compounds collected from the root (exudate
298 sample) and then diluted into liquid media are very unlikely to be present at the same
299 concentrations as those in the experimental pea rhizosphere. In addition, the exact
300 chemical composition of root exudates will also reflect the two different plant growth
301 conditions. Despite these caveats, expression of approx. 80% of the genes selected to
302 make biosensors are elevated by the conditions of the microarray experiments with
303 added root exudate and/or the pea rhizosphere, which suggests that they will be useful
304 in investigating the pea rhizosphere *in situ*.
305 We analyzed *lux* expression on roots *in vivo* with each of the fourteen biosensors
306 in Rlv3841. To ensure that expression of each biosensor is due to chemicals released
307 from the plant roots, each bioreporter was spotted onto FP agar plates (supplemented
308 with pyruvate and ammonium chloride) and incubated for 7 days (no growing plant
309 present). The images (Supplemental Fig. S3) show no luminescence, thus indicating
310 that the inducing compound is coming from the plant roots. To confirm that the
311 biosensors respond to the same inducers on roots (*in vivo*) as they do *in vitro*, flooding
312 experiments were undertaken. Pea roots at 4 dpi with a specific biosensor were flooded
313 with a solution of a compound shown to induce Lux expression *in vitro* (Table I).
314 Inoculation with the xylose, sucrose or GABA biosensor and flooding with xylose,
315 sucrose or GABA, respectively, induced a Lux signal (Supplemental Fig. S4, A-C).
316 Moreover, flooding the sucrose biosensor-inoculated roots with GABA, and the GABA
317 biosensor-inoculated roots with sucrose showed no increase in Lux expression
318 (Supplemental Fig. S4, D-E).
319 Images representative of those obtained on pea roots for the biosensors for sucrose
320 (a sugar), *myo*-inositol (a polyol), malonate (an organic acid) and phenylalanine (an
321 amino acid) are shown in Fig. 2, A-D. Luminescence images revealed that each of these
322 four biosensors detected target metabolites during the 22 dpi period, and the results
323 gave not only the location of the detected compound, but also, by following the same

plant over time, the changes that occur over the course of an experiment. Bearing in mind that the bacterial cells containing the bioreporter need to be metabolically active to generate a Lux signal, it is possible to get a false negative result, i.e. the inducing compound is present at levels above the minimum sensitivity, but the cells do not have the energy required to produce the signal. The signal from a constitutive Lux fusion fades over several days because it places a substantial energy drain on cells. However, if Lux is detected, it indicates the inducing compound is present. Analysis of the localization of luminescence in the images (4 or more plants) and the different temporal patterns of metabolite detection during the colonization and nodulation process (Fig. 2, E-H, Fig. 3) revealed that there were similar detection profiles which could be grouped to aid analysis, although the scale and maximum values observed are different for each bio-reporter.

The biosensor for the polyol, *myo*-inositol (able to detect ≥100 μM *myo*-inositol, Table I), was induced in the rhizosphere, mostly on the primary root and near the tips of lateral roots (Fig. 2, B and F), with a steady decrease in expression over time. Expression of the *myo*-inositol reporter that was seen 15 dpi was mostly in nodules. A similar pattern was seen for the reporters detecting xylose (able to detect ≥ 1 mM xylose), fructose (able to detect ≥ 10 μM fructose) and the flavonoid, hesperetin (able to detect ≥ 1 μM hesperetin) (Fig. 3, A-B and F, Supplemental Fig. S5, A-B and F). Biosensors for these compounds were highly expressed in the rhizosphere at 4-8 dpi, usually localized at and above lateral root tips and then, despite a general decrease in luminescence over the whole root, the compounds were then detected almost exclusively in nodules 15-22 dpi (Supplemental Fig. S5, A-B and F). Expression of the organic acid C4-dicarboxylate biosensor indicated that succinate/malate/aspartate (able to detect ≥ 100 μM/ ≥ 10 μM/ ≥ 10 mM of succinate/malate/aspartate, respectively) are present in the rhizosphere and then found specifically localized to nodules at 15-18 dpi, with levels dropping by 22 dpi (Fig 4D, Supplemental Fig. S5C).

A second expression profile, although similar to that described above, is that of biosensors that gave a strong signal on roots but were barely detectable within nodules. For example, the biosensor for malonate (able to detect ≥ 10 mM malonate) (Fig. 2, C and G) was detected only in the rhizosphere (4-8 dpi), both on primary and lateral roots, with the highest levels appearing just before the root tips (Fig. 2C). The expression of this reporter fell over the time course (Fig. 2G) and was barely detectable in early

nodules (11-15 dpi) and undetectable in older nodules (18-22 dpi) (Fig. 2, C and G).

A third profile, typified by the phenylalanine biosensor (able to detect ≥ 10 μM phenylalanine), showed two peaks of total luminescence (Fig. 2H) similar to that seen with the constitutive promoter (Fig. 1B), one at 8 dpi with the signal localized to the root elongation zone of lateral roots, and a second peak both in the rhizosphere and in nodules (15 dpi) (Fig. 2, D and H). Although the total signal from the phenylalanine reporter detection fell over time, at 18-22 dpi the luminescence was confined to nodules. By following the pattern of luminescence of a number of individual nodules, we conclude that the phenylalanine concentration peaks in nodules and then falls as the nodule senesces. As new nodules are being initiated constantly over the time course analyzed, there were numerous bright spots, which got brighter as the nodule developed and then faded as nodules got older (Fig. 2D). The tartrate sensor (able to detect levels ≥ 100 μM tartrate), was expressed in a temporal pattern similar to that of phenylalanine with a similar dip in total levels of detection as nodules form 11 dpi (Fig. 3D), although, in contrast to the phenylalanine sensor, the tartrate reporter was expressed largely on the primary root (4-15 dpi) (Supplemental Fig. S5D); there may be low levels of expression of the tartrate reporter in mature nodules (22 dpi) (Supplemental Fig. S5D).

A fourth profile was high expression of the reporter in nodules once they are formed, with very weak or no luminescence in the rhizosphere on pea roots in general prior to that. The biosensor for sucrose typifies this group (Fig. 2, A and E). The total levels of expression of the sucrose reporter (able to detect levels ≥ 100 μM sucrose), did not peak until the nodules were more mature (15-18 dpi) and then fell as the nodules senesced (22 dpi) (Fig. 2E). In the same way, expression of the GABA reporter (able to detect levels ≥ 500 μM GABA), was hardly detected in the rhizosphere, but was induced specifically in nodules, with total levels peaking at 15-18 dpi (Fig. 3E, Supplemental Fig. S5E).

The fifth profile was seen with a group of biosensors that gave results too low to properly evaluate, because luminescence was routinely detected below a mean intensity *per* pixel of approx. 30 (Supplemental Fig. S6). The polyol reporters for erythritol (able to detect levels ≥ 1 mM erythritol), and mannitol (able to detect levels ≥ 1 μM mannitol), were barely detected in either the rhizosphere or in nodules of pea plants (Supplemental Fig. S6, A-B). The reporter for formate (able to detect levels ≥ 10 mM formate), was expressed at very low levels and expression of the salicylic acid reporter

(able to detect levels ≥ 1 mM salicylate), was not detectable (Supplemental Fig. S6, C-D). This last result is not unexpected, because formate and salicylic acid were not found in the metabolomic analysis of pea root exudate (Supplemental Table S3).

Based on the spatial localization on pea roots of the reporters, we can draw conclusions about metabolites found in the rhizosphere prior to nodule formation (Table III). Xylose (≥ 1 mM), fructose (≥ 10 μM), *myo*-inositol (≥100 μM), phenylalanine (≥ 10 μM) and hesperetin (≥ 1 μM) are largely exuded by the elongation zone of primary and lateral roots (Fig. 2, B and D, Supplemental Fig. S5, A-B and F). Malonate (≥ 10 mM) was detected on both the uppermost portion of the primary root and the elongation zone of primary and lateral roots (Fig. 2C). Tartrate (≥ 100 μM) exudation was exclusively localized to the uppermost portion of the primary root, with little or no tartrate being detectable on the lateral roots (Supplemental Fig. S5D). Although present in the pea rhizosphere, the localization of C4-dicarboxylates was not clear, because detection in different regions varied over time with no clear pattern being observed (Supplemental Fig. S5C).

Between 11 and 15 dpi nodules became visible on pea roots. The reporters indicate that xylose (≥ 1mM), fructose (≥ 10 μM), sucrose (≥ 100 μM), *myo*-inositol (≥ 100 μM), C4-dicarboxylates (≥ 10 μM -10 mM, see Table I), phenylalanine ((≥ 10 μM), GABA (≥ 500 μM) and hesperetin (≥ 10 μM) were present in nodules at 15 dpi (Table III, Fig. 2 A, B, D-F, and H, Fig. 4 B-E, and Supplemental Fig. S7). Malonate (≥ 10 mM), and tartrate (≥ 100 μM), were detectable in nodules at 15 dpi, but at very low levels of bio-reporter expression (towards the lower limit of detection) (Table III, Fig. 2 C and G, and Supplemental Fig. S5D). For both phenylalanine and hesperetin, levels were highest in nodules at 15 dpi (dropping to 18 dpi, and dropping further to 22 dpi) (Table III, Supplemental Fig. S5F, and Supplemental Fig. S7, C-D). In most of the biosensors, the signal from nodules was strongly reduced by 22 dpi probably due to the general plant growth conditions, the only exception being the fructose reporter where the signal increased until 22 dpi (Table III and Supplemental Fig. S7B).

Effect of Nodulation on Rhizosphere Metabolites

Since wild-type Rlv3841 induces nodule formation on pea roots, the effects of nodulation on pea root secretion were investigated by comparing the induction of the biosensors in wild-type with their induction in a mutant unable to induce nodulation (a

derivative of Rlv3841 carrying *nodC128*::Tn*5* (Downie et al., 1985)). Rhizobia produce Nod factors enabling recognition by legumes, and *nodC* mutants are unable to enter the plant or induce nodule formation (Udvardi and Poole, 2013). By comparing results obtained with wild-type and mutant backgrounds it is possible to separate the processes and metabolite changes of root colonization and nodule formation (Fig. 2 and 4, Supplemental Fig. S5, S8 and S9). Notably, in the pre-nodule formation stage, 4-8 dpi, no significant differences occurred between any biosensor in the two different backgrounds, other than with the *myo*-inositol reporter 8 dpi (Fig. 2F). This suggests that the presence of Nod factor in itself does not alter either the amount or the localization of root secretions prior to nodule formation for the sugars xylose, fructose, and sucrose, the organic acids malonate, C4-dicarboxylates, and tartrate or the amino acids phenylalanine, and GABA.

With the *nodC* mutant that is unable to form nodules, there was a significant decrease in detection of *myo*-inositol at 8 dpi relative to wild-type (Fig. 2F). In a wild-type strain at this time point, nodule initiation has begun, although nodules are not yet visible to the naked eye. The conclusion that *myo*-inositol (at concentrations $\geq$ 100 μM) is present in developing and very young nodules can be drawn from the relative decrease in *lux* expression of *myo*-inositol biosensor on roots inoculated with the *nodC* mutant. There was also a significant decrease in expression of the *myo*-inositol reporter in roots inoculated with the *nodC* mutant at each time point from 8 to 18 dpi, suggesting the *myo*-inositol detected in the roots inoculated with wild-type is due to nodule formation (Fig. 2F). Indeed, expression of the *myo*-inositol reporter can be seen clearly localized to nodules (Fig. 2B). Lux output from the sucrose reporter (detecting concentrations $\geq$ 100 μM sucrose), was reduced significantly at 11-22 dpi in roots inoculated with the *nodC* mutant compared with wild-type (Fig. 2E); the expression of this reporter in roots inoculated with Rlv3841 was clearly seen localized to nodules at 15-22 dpi and this is consistent with sucrose from the shoot being supplied to nodules to support nitrogen fixation by rhizobial bacteroids (Fig. 2A). Expression of the phenylalanine reporter (detecting concentrations of $\geq$ 10 μM phenylalanine), was reduced significantly only at 15 dpi in roots inoculated with the *nodC* mutant compared to wild-type (Fig. 2H), suggesting phenylalanine is abundant in nodules of this age. For fructose, C4-dicarboxylates, GABA, and hesperetin bioreporters, levels are significantly lower in the *nodC* mutant background at 18 dpi, 15 dpi, 15 and 18 dpi, and

18 dpi, respectively (Fig. 3, B-C, and E-F), indicating the presence of these metabolites (fructose ≥ 10 μM, C4-dicarboxylates ≥ 10 μM – 10mM, GABA ≥ 500 μM, hesperetin ≥ 1 μM) in pea nodules.

Effect of Symbiotic Nitrogen Fixation on Nodule Metabolites

Biosensors detecting sucrose (sugar), *myo*-inositol (polyol), C4-dicarboxylates (organic acid) and GABA (amino acid) were used to examine levels of metabolites within effective and ineffective nodules by transferring each to a *nifH* mutant background (Karunakaran et al., 2009). The *nifH* mutant induces normal nodule formation, but is totally defective for nitrogen fixation. Since *nifH* encodes one of the components of nitrogenase, the enzyme complex that carries out nitrogen fixation, interruption of this gene by mutation means no functional nitrogenase is produced by the bacteria.

Levels of Lux expression from a constitutive promoter were approx. 30% lower in the Rlv3841 *nifH* mutant background relative to wild-type (Fig. 4A), presumably because ineffective nodules do not contain as many, and/or as metabolically active, bacteroids. Levels of detection of sucrose, *myo*-inositol, C4-dicarboxylates and GABA in effective (wild-type) and ineffective (*nifH* mutant-background) nodules were compared 15, 18, and 22 dpi (Fig. 4, B-E). Once corrected for overall lower activity in the *nifH*-mutant background (Supplemental Fig. S10), lower levels of sucrose (approx. 65% at 15 dpi, approx. 35% at 18 dpi), C4-dicarboxylates (approx. 35% at 15-18 dpi, > 10% at 22 dpi), and GABA (approx. 65% at 15 dpi, approx. 30% at 18 dpi and approx. 50% at 22 dpi) were detected in ineffective nodules. The reduction of sucrose, C4-dicarboxylates and GABA in ineffective nodules suggests that plants sanction nodules that cannot fix nitrogen by decreasing their carbon supply (Fig. 4, B, and D-E). In contrast, the level of *myo*-inositol detected was higher in ineffective senescing nodules at 22 dpi (approx. 600% at 22 dpi) (Fig. 4C, Supplemental Fig. S10).

Malonate catabolism is not required for nitrogen fixation (Karunakaran et al., 2013). Transcriptomic data did not show a significant change in the expression of *matABC* genes in the rhizosphere of pea plants, but a significant difference was found in the alfalfa rhizosphere (Ramachandran et al., 2011). The malonate biosensor indicates that malonate (at concentrations ≥ 10 mM) is present in the pea rhizosphere, although over time its level decreases to being barely detectable in nodules 15 dpi (Fig. 2, C and G). With evidence that ≥ 10 mM malonate is present in the rhizosphere of

peas, colonization of roots by *R. leguminosarum* mutants defective for malonate metabolism was explored to see if an inability to metabolize malonate affects this process. Root attachment assays and nodule competition (as a measure of effective root colonization) were assayed using *matC* and *matA* mutants that are impaired in malonate transport and catabolism, respectively (Karunakaran et al., 2013). Although both mutants, defective in either malonate transport or catabolism, are less efficient at root attachment than the wild-type, there were no significant differences in pea root colonization compared with wild-type (Supplemental Fig. S11). We conclude from this that malonate uptake and its subsequent bacterial catabolism play a part in the initial attachment of *R. leguminosarum* to pea roots. However, although attachment might be the first step of bacterial colonization, in overall colonization assays, ability to either take-up or metabolize malonate has no effect.

In vivo Mapping of Metabolites on Roots and within Nodules of *V. hirsuta*

To investigate a different legume root and its rhizosphere, similar analyses were performed with *V. hirsuta,* on which Rlv3841 is also able to form nodules. Images were acquired at similar time points as for pea (up to 22 dpi), but with vetch plants the nodules appear to the naked eye earlier, at about 8 dpi (Fig. 5 and Table IV). With the exception of the polyols, erythritol and mannitol, and the organic acids, formate, tartrate and salicylic acid, all other metabolite were detected in the vetch rhizosphere over the time course (Table IV). For the compounds we failed to detect, we can't exclude the possibility that they may be present, but at levels too low for their detection, i.e. levels of erythritol at ≤ 1 mM, mannitol at ≤ 1 μM, formate at ≤ 10 mM, tartrate at ≤ 100 μM and salicylic acid at ≤ 1 mM. This differs from pea only in the case of the tartrate, which was detected in the pea rhizosphere but not in that of vetch. Metabolites xylose (≥ 1 mM), fructose (≥ 10 μM), *myo*-inositol (≥ 100 μM), malonate (≥ 10 mM), C4-dicarboxylates (≥ 10 μM -10 mM, Table I), and hesperetin (≥ 1 μM) were detected in the vetch rhizosphere at 4 dpi (Fig. 5, A-B, D-F, and I). These were also all detected on pea roots (Table III), but a difference between these two legume rhizospheres is that phenylalanine was barely detected in the vetch rhizosphere at 4 dpi (Fig. 5G) (the limit of detection is ≥ 10 μM phenylalanine). In vetch, as in pea, sucrose (able to detect ≥ 100 μM), and GABA (able to detect (≥ 500 μM) were hardly detected on the roots prior to nodule formation but were detected within nodules: for sucrose, the maximum level was observed at 11 dpi, while that of GABA peaked at 8 dpi (Fig. 5, C and H). This

pattern is similar overall to that seen on pea roots for both sucrose (Fig. 2E) and GABA (Fig. 3E), taking into account that pea nodules form later (>11 dpi). Malonate (≥ 10 mM) was detected in the vetch rhizosphere prior to nodule formation, but once nodules were formed (> 8 dpi), it was detected only at a very low level (8-22 dpi) (Fig. 5E), again, a similar pattern to that of pea (Fig. 2G). Hesperetin (≥ 1 μM) was detected in vetch, with levels peaking at 4 dpi, and then falling once nodule development was initiated (8 dpi onwards) (Fig. 5I). Images from 1-22 dpi for detection of hesperetin on vetch roots (Fig. 6) show that, even at 1-4 dpi, prior to any sign of nodule formation, there are foci where hesperetin is detected. At later time points, nodules developed at these exact locations illustrating the power of this technique in pinpointing the spatial and temporal secretion of this flavonoid (Fig. 6).

DISCUSSION

Owing to the hidden nature of the rhizosphere and its complexity, a major problem encountered in its study is the intrinsic difficulty in sampling (Bais et al., 2006). Most of the techniques used require either sacrifice of the specimen, or at least require its manipulation, making it impossible to non-invasively follow the same sample over time. The bacterial *lux* gene cassette has been widely used in several different applications, including the visualization of gene expression, as a tool for cellular population monitoring and as bioreporter target through activation under specific, predetermined conditions (Close et al., 2012). In this work, we have constructed a suite of Lux biosensors able to detect a variety of key sugars, polyols, organic acids, amino acids and flavonoids that are commonly found in root exudates. The presence of these compounds was confirmed using a metabolomics approach, allowing us to identify 376 compounds present in pea root exudate. Lux-based reporter plasmids have been transferred into Rlv3841, an alpha-proteobacterium, which is generally associated with leguminous plants and is ubiquitous in soil (Udvardi and Poole, 2013). Pea and vetch plants, both hosts of *R. leguminosarum,* on which it forms nitrogen-fixing nodules, have been used to test the efficiency of this system as a proof-of-concept. However, the ability of rhizobia to colonize non-legume plants (Chabot et al., 1996) should allow the use of these bioreporters in other systems.

A constitutive promoter was used to examine rhizobial colonization of plant roots. Bacteria colonize the whole of the root system but the strongest Lux signals are

visible from the elongation zone of the primary and lateral roots (Fig. 1, Supplemental Fig. S2). Heavy colonization at the root elongation zone is to be expected, as this is an area of actively growing root where many metabolites are secreted and exuded. Low Lux signal from the root cap is probably due to the reduced colonization of this area, which generally secretes antimicrobial phytochemicals (Baetz and Martinoia, 2014). The level of Lux signal detected in the rhizosphere was constant until 11 dpi and then reduced, possibly due to a general decrease in root exudation caused by plant growth conditions and/or to the physiological status of the bacterial population. Constitutive *lux* expression drains energy reserves in bacterial cells and reduces the light output over time. In a wild-type bacterial background, after 11 dpi the Lux signal was mainly localized in the nitrogen-fixing nodules formed on the legume roots which is densely populated with metabolically active bacteria. It is important to consider where bacteria are located. Although the whole root is colonized by rhizobia (Figure S2), these are unevenly distributed i.e. more bacteria or more metabolically active bacteria are in the root elongation zone. The overall levels of metabolites detected in the rhizosphere before 11 dpi and in nodules (after 11 dpi) for pea roots are summarized in Fig. 7.

On pea and vetch roots, xylose (≥ 1 mM), fructose (≥ 10 μM), *myo*-inositol (≥ 100 μM), phenylalanine (≥ 10 μM) (not detected in the vetch rhizosphere), and hesperetin (≥ 1 μM) were detected largely at the elongation zone (just behind the root tip) of lateral roots, while malonate (≥ 10 mM) (at least initially) and tartrate (≥ 100 μM) (not detected on vetch roots) were mainly localized on the primary root (Fig. 2C and Supplemental Fig. S5D). In Rlv3841, malonate transport and metabolism has been shown to have no role in nitrogen fixation in peas (Karunakaran et al., 2013), but does seem to be involved in attachment of Rlv3841 to pea roots as mutants in malonate uptake and metabolism show a reduced attachment phenotype, although no change in overall colonization of pea roots is observed. Malonate at ≥ 10 mM is localized to the primary root at 4 dpi during initial colonization (although levels of ≤ 10 mM malonate may well be present on other parts of the root but are below the levels of detection by this method). Given the role of malonate in attachment, it is possible that bacteria attach to the primary root before colonizing the lateral roots, where most of the nodules subsequently appear. C4-dicarboxylates (succinate/malate/aspartate with detection levels ≥ 100 μM/ ≥ 10 μM/ ≥ 10 mM, respectively) were detected in the rhizosphere of both pea and vetch, but showed no clear spatial pattern on pea roots (Supplemental Fig.

588 3C).

589 In pea and vetch nodules, xylose (≥ 1 mM), fructose (≥ 10 μM), sucrose (≥ 100
590 μM), *myo*-inositol (≥ 100 μM), C4-dicarboxylates (succinate/malate/aspartate, (≥ 10
591 μM – 10 mM), phenylalanine (≥ 10 μM), and GABA (≥ 500 μM) were present (Table
592 III, Table IV, Fig. 7). Although nodules formed on pea and vetch have not been
593 analyzed by metabolomic studies, MALDI mass spectrometric analysis of *Medicago*
594 *truncatula* nodules formed by *S. meliloti* (Ye et al., 2013) revealed many of these same
595 compounds present: sucrose, C4-dicarboxylates (succinate/malate/ aspartate), and
596 GABA, but also salicylic acid was detected, which, if present in pea or vetch nodules,
597 is below the limits of detection (≤ 1 mM) of Lux-based salicylic acid detection. In pea,
598 hesperetin (≥ 1 μM) was detected in mature nodules (Fig. 3F), while in vetch it was
599 detected only before nodules could be seen with the naked eye or in very young nodules,
600 with none detected in mature nodules (i.e. levels ≤ 1 μM) (Fig. 6). Sucrose is supplied
601 from the shoot to nodules, where it is converted to C4-dicarboxylates and supplied to
602 bacteroids as their primary energy source for nitrogen fixation (Poole and Allaway,
603 2000). In the ineffective nodules of a *nifH*-mutant background, the levels of sucrose
604 and C4-dicarboxylates detected were lower, suggesting that the plant sanctions supply
605 of carbon to nodules unable to provide them with nitrogen. While the *nifH*-mutant
606 showed lower levels of the constitutive promoter, presumably because of reduced
607 bacteroid numbers and metabolic activity, (Kiers et al., 2003; Berrabah et al., 2015),
608 the levels of sucrose, C4-dicarboxylates and GABA were still substantially reduced
609 when the decrease in activity of the constitutive promoter was accounted for.
610 Furthermore, levels of some metabolites, such as *myo*-inositol, increased dramatically
611 in the *nifH* mutant possibly due to environmental/osmotic stress.

612 Use of these tools has allowed us to draw a spatial and temporal map of key
613 compounds present in the legume rhizosphere and to monitor the relative supply of
614 specific metabolites inside nodules (e.g. sucrose, C4-dicarboxylates, GABA). We have
615 demonstrated that with this system it is possible to follow the same plant for days,
616 gathering data non-invasively and it is relatively easy to set up. Moreover, it will be
617 possible in the future to expand the set of reporters to include many different
618 compounds. We believe that this is an excellent tool, which can be adapted to
619 investigate the role of specific root exudates in many different plant growth conditions
620 (e.g. stress; both abiotic and biotic). As *R. leguminosarum* spp. colonize root systems

of non-leguminous plants (Schloter et al., 1997), it will be possible to monitor root exudates of other plant species using this series of biosensors. By combining this methodology with plant mutant collections, screening specific exudate-related phenotypes in genome-wide association studies could be performed. Finally, by co-inoculating biosensors with other bacteria and/or fungi, it will be possible to observe the effects of other microorganisms on the plant secretome.

MATERIALS AND METHODS

Bacterial Strains and Growth Conditions

The bacterial strains and plasmids used in this study are listed in Supplemental Table S1. *Escherichia coli* strains were grown in liquid or solid Luria–Bertani (LB) medium (Sambrook et al., 1989) at 37°C supplemented with appropriate antibiotics: tetracycline (10 μg ml^{-1}) and kanamycin (20 μg ml^{-1}). Rlv3841 carrying *nodC128*::Tn5 was isolated by transduction using phage RL38 propagated on strain 6015 carrying *nodC128*::Tn5 on pRL1JI (Downie et al., 1985). Rlv3841 strains were grown in tryptone yeast (TY) agar or broth (Beringer, 1974) or universal minimal salts (UMS) at 28°C. UMS is derived from AMS (Poole et al., 1994) with the changes being: EDTA-Na_2 (1 μM), $CoCl_2.6H_2O$ (4.2 μM), $FeSO_4.7H_2O$ (0.04 mM) and $CaCl_2.2H_2O$ (0.51 mM); UMS was supplemented with 30 mM pyruvate and 10 mM ammonium chloride as the carbon and nitrogen sources, unless otherwise stated (Supplemental Table S2). UMA is UMS with the addition of 16 g l^{-1} agar. Antibiotics were added when necessary at the following concentrations: streptomycin (500 μg ml^{-1}), tetracycline (2 μg ml^{-1} in UMS, 5 μg ml^{-1} in TY), spectinomycin (100 μg ml^{-1}) and neomycin (20 μg ml^{-1}).

Strain Construction and General Techniques

The promoter region (often including the complete upstream regulator) of each of the candidate genes was amplified using primers listed in Supplemental Table S9 with Phusion High-Fidelity DNA Polymerase (ThermoFischer, Waltham, MA, USA) according to manufacturer's instructions. Fragments were purified and double digested with *Kpn*I or *Xho*I (at the 5′-end) and *Xho*I or *Bam*HI (at the 3′-end) (ThermoFischer). Restriction fragments were cloned into pIJ11268 (Frederix et al., 2014) digested with

653 the same enzymes. Plasmids (Supplemental Table S1) were transferred into wild-type
654 (Rlv3841), Rlv3841 *nodC128*::Tn5, Rlv3841 *nifH*::ΩSp (Karunakaran et al., 2009),
655 Rlv3841 *matA*::pK19 and Rlv3841 *matC*::pK19 (Karunakaran et al., 2013)
656 backgrounds by tri-parental mating according to Figurski and Helinski (Figurski and
657 Helinski, 1979). All plasmids are available from addgene (https://www.addgene.org).
658
659 **Determining Solute Specificity**
660 Each biosensor was grown for 3 d on an UMA slope with antibiotics, re-suspended in
661 UMS with no added carbon or nitrogen and washed three times. Each was then diluted
662 to an OD_{600} of 0.01 in a final volume of 5 ml UMS with a sugar (10 mM) as sole carbon
663 source, or with pyruvate (30 mM) as carbon source in presence of a specific compound
664 (Supplemental Table S2) for 17 h. Luminescence (in relative luminescence units
665 (RLU)) and OD_{600} were measured using a GloMax®-Multi+ Detection System
666 (Promega, Fichburg, WI, USA). For each compound, the fold-induction is defined as
667 the ratio of RLU/OD_{600}, when grown in the presence of that compound (Supplemental
668 Table S2 gives concentrations of each solute), with that obtained in control conditions
669 (UMS with pyruvate and ammonia). The solute(s) that give the highest fold-induction
670 and specific luminescence (Table I) are described as inducer(s). Biosensor induction by
671 a solute is described as specific if the specific luminescence is ≥10-fold that observed
672 from the other solutes tested. The biosensors for erythritol, formate, and GABA have a
673 relatively high expression with a variety of non-related solutes (background) and they
674 are described as being specific for these solutes, respectively, with specific
675 luminescence ≥4-fold values obtained with other solutes. More than one compound is
676 considered inducing when the fold-induction is > 40% of the maximum fold-induction
677 for a biosensor (Table I). For each biosensor grown on each solute, three independent
678 cultures were measured. Supplemental Table S10 shows the expression of each gene
679 used in biosensor construction in microarray experiments performed under seventy-
680 three different conditions.
681
682 **Plant Growth Conditions**
683 Seeds of *Pisum sativum* cv Avola and *Vicia hirsuta* were surface sterilized and
684 germinated on distilled water agar plates. Plates with pea seedlings were put into black
685 bags and incubated for 6 d at room temperature. Vetch seedlings were incubated
686 overnight at 4°C and for 3 d at room temperature. Seedlings were transferred to 10-cm

687 square Petri dishes containing FP agar (Somasegaran and Hoben, 1994) covered with
688 sterile filter paper (one seedling per plate for peas, six per plate for vetch). Each
689 biosensor was analyzed with at least 4 plates for pea (corresponding to 4 plants) and 1
690 plate for vetch (corresponding to 6 plants). Biosensors were grown on UMA slopes for
691 3 d at 27°C, washed 3 times in UMS without any additions and inoculated directly on
692 the seedling root. Each seedling was inoculated with 5 x 10^7 or 2 x 10^7 colony forming
693 units (cfu), for vetch and pea plants, respectively. Plates were covered with aluminum
694 foil to prevent exposure of roots to light and placed in a growth chambers at 23°C with
695 a 16 h/8 h day/night for 22 d. In flooding experiments, peas were grown for 4 dpi with
696 a biosensor before the plate was flooded with 10 ml of 10 mM solution of substrate and
697 poured off. Plates were imaged before, and 5 min, 3 hr, and 21 hr post-flooding.
698 Background luminescence in experiments with plants was evaluated by spotting 2 x 10^7
699 cfu ml^{-1} bacteria (the same amount used for pea root inoculation) onto FP plates
700 supplemented with pyruvate and ammonium chloride. Plates were imaged after 7 d.
701
702 **Image Acquisition**
703 Plates were photographed using a NightOWL camera (Berthold Technologies,
704 Bad Wildbad, Germany) 4, 8, 11, 15, 18, and 22 d post inoculation (dpi). CCD images
705 of light output were exposed for 120 s. Each CCD image consisted of an array 1024 by
706 1024 pixels, and after acquisition pictures were post-processed for cosmic suppression
707 and background correction. Images were analyzed with the imaging software IndiGO
708 (Berthold Technologies) and with the custom software, NightCROP. NightCROP first
709 segments an image using the SeNeCA algorithm (Tomek et al., 2013) into roots and
710 background using a bright-field image, discarding objects smaller than 1000 pixels. All
711 subsequent analysis uses the respective fluorescence image. The script subtracts
712 background intensity: background in the image is defined as a set of pixels given by
713 logical inverse of the mask containing roots, subsequently morphologically eroded with
714 a disk structural element of radius 9 to filter out signal from the edges of roots. Then,
715 for each pixel belonging to a root, mean intensity of background pixels in a 200-by-
716 200-pixel square is subtracted. The output from NightCROP for a given image is
717 expressed as mean intensity of pixels labeled as roots after the background subtraction.
718 Exact values of parameters (minimum root size, erosion radius and background size)
719 may be freely selected, based on the resolution and nature of data (Fig. S1). Data are

720 expressed as the ratio of luminescence/surface; cps mm^{-2} (counts per second mm^{-2};
721 IndiGO) or intensity pxl^{-1} (NightCROP).
722
723 **Software Development and Use**
724 NightCROP was developed as a script for MATLAB environment (MATLAB
725 version 8.5.0 r2015a, (MathWorks Inc., Natick, MA, USA)). Before using the script an
726 image processing toolbox should be installed in MATLAB. The script is available upon
727 request to the corresponding author and works on any operating system which supports
728 MATLAB.
729
730 **Extraction of Exudate from Roots**
731 Glass jars (0.5 l) were prepared by filling one third of the jar with glass beads
732 (6 mm diameter; Atlas Ball & Bearing Co. Ltd., Walsall, UK) and adding water (reverse
733 osmosis highest quality) to cover all except the top layer of beads (approx. 150 ml).
734 Jars were covered with a metal lid containing a foam bung and sterilized by autoclaving.
735 Six sets of twenty sterilized and germinated peas with 1 cm roots were transferred into
736 six sterilized glass jars, with each jar (of twenty plants) representing one biological
737 replicate. The jars were wrapped with black plastic up to the level of the beads and the
738 peas grown for 21 d at 20°C for 16 h light /18°C for 8 h dark. The liquid was then
739 decanted into sterile glass bottles and sampled for sterility by plating 100 µl aliquots on
740 TY plates. Samples were filtered through a 0.2-µm nitrocellulose filter. Samples for
741 metabolite profiling were freeze- dried and re-suspended in 800 µl of sterile water prior
742 to downstream analysis.
743
744 **Metabolite Profiling Analysis**
745 The metabolomic profile of six biological replicates of pea root exudates was
746 analyzed using non-biased, global metabolome profiling technology based on GC/MS
747 and UHLC/MS/MS^2 platforms (Lawton et al., 2008; Evans et al., 2009; Terpolilli et al.,
748 2016) developed by Metabolon (www.metabolon.com). Samples from the six
749 biological replicates were extracted using the automated MicroLab STAR® system
750 (Hamilton, www.hamiltoncompany.com). Recovery standards (Evans et al., 2009)
751 were added prior to the first step in the extraction process for QC purposes. The protein
752 fraction was removed using methanol extraction, which allows maximum recovery of
753 small molecules. The resulting extract was divided into two fractions: one for analysis

754 by LC and one for analysis by GC. Organic solvent was removed by placing samples
755 on a TurboVap® (Zymark). Each sample was frozen and dried under vacuum. Samples
756 were then prepared for the appropriate instrument, either LC/MS or GC/MS.
757 The LC/MS portion of the platform was based on a Waters ACQUITY UHPLC
758 and a Thermo-Finnigan LTQ mass spectrometer, which consisted of an electrospray
759 ionization source and linear ion-trap mass analyzer. The sample extract was split into
760 two aliquots, dried and then reconstituted in acidic or basic LC-compatible solvents,
761 each of which contained 11 or more injection standards at fixed concentrations. One
762 aliquot was analyzed using acidic positive ion optimized conditions and the other using
763 basic negative ion optimized conditions in two independent injections using separate
764 dedicated columns. Extracts reconstituted in acidic conditions were gradient-eluted
765 using water and methanol both containing 0.1% (v/v) formic acid, while the basic
766 extracts, which also used water/methanol, contained 6.5 mM NH_4HCO_3. The MS
767 analysis alternated between MS and data-dependent MS^2 scans using dynamic
768 exclusion.
769 Samples destined for GC/MS analysis were re-dried under vacuum desiccation
770 for a minimum of 24 h prior to being derivatized under dried nitrogen using
771 bistrimethyl-silyl-triflouroacetamide. The GC column was 5% phenyl and the
772 temperature ramp was 40°C to 300°C, over a 16-min period. Samples were analyzed
773 on a Thermo-Finnigan Trace DSQ fast-scanning single-quadrupole gas chromatograph
774 mass spectrometer using electron impact ionization. For metabolite profiling,
775 identification of known chemical entities was based on comparison to metabolomic
776 library entries of purified standards as previously described (Evans et al., 2009; Yobi
777 et al., 2012).
778
779 **RNA Isolation and Microarray Analysis**
780 Rlv3841 was grown overnight in 10 ml of UMS supplemented with
781 pyruvate/ammonia. Cultures were split in two and concentrated root exudates (5 mg/ml)
782 were added to one culture. After 3 h of induction RNA was extracted from three
783 biological replicates, amplified and hybridized as previously described (Karunakaran
784 et al., 2009). Microarray data were deposited in the ArrayExpress database
785 (www.ebi.ac.uk/arrayexpress) under accession number E-MTAB-4790.
786
787 **Root Attachment Assay**

Surface-sterilized pea seeds were germinated on distilled water agar plates for 5 d. Bacteria were grown on UMA slopes for 3 d, re-suspended and washed twice in phosphate-buffered saline and then 10 ml of a suspension (OD_{600} = 0.1) was added to 50 ml glass tubes containing 7-10 pea roots. Tubes were incubated on a rocking platform for 1 h at room temperature at 50 rpm. Roots were washed by dipping six times in PBS and then individual roots were transferred into a 1.5 ml tube, weighed and their luminescence measured using a GloMax®-Multi Jr Single-Tube Multimode Reader (Promega). Luminescence was scored as relative light units. Data are the average of individual roots from at least 3 different experiments; relative light units (RLU) were normalized for the weight of the roots and the average luminescence of roots incubated with bacteria not expressing the *lux* cassette (LMB542) was subtracted. Luminescence of the pure culture after 1 h was used to calculate the relative luminescence of a single bacterial cell. Differences between the three groups were calculated by one-way ANOVA with post hoc Tukey test.

Root Competition Assay

Pea plants were grown on FP plates as described above (Plant Growth Conditions), with the addition of a wet filter paper to cover the roots. Strains were co-inoculated in 1:1 ratio (1 x 10^7 cfu of each strain), using combinations of Rlv3841 with either Rlv3841 [pIJ11282] or Rlv3841 *matC*::pK19 [pIJ11282] and Rlv3841 *matC*::pK19, with either Rlv3841[pIJ11282] or Rlv3841 *matC*::pK19 [pIJ11282]. At 7 dpi, plants were imaged using a NightOWL camera and processed using the NightCROP script.

Biosensor Sensitivity Assay

Bacterial biosensors from UMA slopes (with appropriate antibiotics) grown for 3 d at 28˚C, were washed three times before re-suspension in 3 ml UMS. Bacteria were added to 50 ml of molten (cooled to 42˚C) UMA, to give a final concentration of 1x 10^8 cfu ml^{-1}. The agar containing bacteria was then poured into a 12-cm square Petri dish and allowed to set. 25 µl droplets (n=5) of 10-fold dilutions of solute, concentrations ranging from 10 mM to 1 µM (including a distilled water control) were spotted onto the agar and incubated at 28˚C. Sensitivity of each biosensor was defined as the lowest

concentration of solute which gave a signal when imaged using a NightOWL camera at 4 h post-spotting.

ACKNOWLEDGEMENTS

We would like to acknowledge the technical assistance of Elisabeth Nowak in this work.

Literature Cited

Badri DV, Weir TL, van der Lelie D, Vivanco JM (2009) Rhizosphere chemical dialogues: plant-microbe interactions. Curr Opin Biotechnol **20:** 642-650

Baetz U, Martinoia E (2014) Root exudates: the hidden part of plant defense. Trends Plant Sci **19:** 90-98

Bais HP, Weir TL, Perry LG, Gilroy S, Vivanco JM (2006) The role of root exudates in rhizosphere interactions with plants and other organisms. Annu Rev Plant Biol **57:** 233-266

Beringer JE (1974) R factor transfer in Rhizobium leguminosarum. J Gen Microbiol **84:** 188-198

Berrabah F, Ratet P, Gourion B (2015) Multiple steps control immunity during the intracellular accommodation of rhizobia. J Exp Bot **66:** 1977-1985

Biedrzycki ML, Bais HP (2009) Root secretions: from genes and molecules to microbial associations. J Exp Bot **60:** 1533-1534

Chabot R, Antoun H, Kloepper JW, Beauchamp CJ (1996) Root colonization of maize and lettuce by bioluminescent Rhizobium leguminosarum biovar phaseoli. Appl Environ Microbiol **62:** 2767-2772

Close D, Xu T, Smartt A, Rogers A, Crossley R, Price S, Ripp S, Sayler G (2012) The evolution of the bacterial luciferase gene cassette (lux) as a real-time bioreporter. Sensors (Basel) **12:** 732-752

Darwent MJ, Paterson E, McDonald AJ, Tomos AD (2003) Biosensor reporting of root exudation from Hordeum vulgare in relation to shoot nitrate concentration. J Exp Bot **54:** 325-334

Downie JA, Knight CD, Johnston AWB, Rossen L (1985) Identification of genes and gene products involved in the nodulation of peas by Rhizobium leguminosarum. Molecular and General Genetics **198:** 255-262

Evans AM, DeHaven CD, Barrett T, Mitchell M, Milgram E (2009) Integrated, nontargeted ultrahigh performance liquid chromatography/electrospray ionization tandem mass spectrometry platform for the identification and relative quantification of the small-molecule complement of biological systems. Anal Chem **81:** 6656-6667

Figurski DH, Helinski DR (1979) Replication of an origin-containing derivative of plasmid RK2 dependent on a plasmid function provided in trans. Proc Natl Acad Sci U S A **76:** 1648-1652

Frederix M, Edwards A, Swiderska A, Stanger A, Karunakaran R, Williams A, Abbruscato P, Sanchez-Contreras M, Poole PS, Downie JA (2014) Mutation of praR in Rhizobium leguminosarum enhances root biofilms, improving nodulation competitiveness by increased expression of attachment proteins. Mol Microbiol **93:** 464-478

Galardini M, Brilli M, Spini G, Rossi M, Roncaglia B, Bani A, Chiancianesi M, Moretto M, Engelen K, Bacci G, Pini F, Biondi EG, Bazzicalupo M, Mengoni A (2015) Evolution of intra-specific regulatory networks in a multipartite bacterial genome. PLoS Comput Biol **11:** e1004478

Huang X-F, Chaparro JM, Reardon KF, Zhang R, Shen Q, Vivanco JM (2014) Rhizosphere interactions: root exudates, microbes, and microbial communities. Botany **92:** 267-275

Kaiser C, Kilburn MR, Clode PL, Fuchslueger L, Koranda M, Cliff JB, Solaiman ZM, Murphy DV (2015) Exploring the transfer of recent plant photosynthates to soil microbes: mycorrhizal pathway vs direct root exudation. New Phytol **205:** 1537-1551

Karunakaran R, East AK, Poole PS (2013) Malonate catabolism does not drive N(2) fixation in legume nodules. Applied and Environmental Microbiology **79:** 4496-4498

Karunakaran R, Ramachandran VK, Seaman JC, East AK, Mouhsine B, Mauchline TH, Prell J, Skeffington A, Poole PS (2009) Transcriptomic analysis of Rhizobium leguminosarum biovar viciae in symbiosis with host plants Pisum sativum and Vicia cracca. J Bacteriol **191:** 4002-4014

Kiers ET, Rousseau RA, West SA, Denison RF (2003) Host sanctions and the legume-rhizobium mutualism. Nature **425:** 78-81

Lawton KA, Berger A, Mitchell M, Milgram KE, Evans AM, Guo L, Hanson RW, Kalhan SC, Ryals JA, Milburn MV (2008) Analysis of the adult human plasma metabolome. Pharmacogenomics **9:** 383-397

Maj D, Wielbo J, Marek-Kozaczuk M, Skorupska A (2010) Response to flavonoids as a factor influencing competitiveness and symbiotic activity of Rhizobium leguminosarum. Microbiol Res **165:** 50-60

893 **Mauchline TH, Fowler JE, East AK, Sartor AL, Zaheer R, Hosie AH, Poole PS,**
894 **Finan TM** (2006) Mapping the Sinorhizobium meliloti 1021 solute-binding
895 protein-dependent transportome. Proc Natl Acad Sci U S A **103:** 17933-17938
896 **Maxwell CA, Hartwig UA, Joseph CM, Phillips DA** (1989) A Chalcone and Two
897 Related Flavonoids Released from Alfalfa Roots Induce nod Genes of
898 Rhizobium meliloti. Plant Physiol **91:** 842-847
899 **Mooney SJ, Pridmore TP, Helliwell J, Bennett MJ** (2011) Developing X-ray
900 Computed Tomography to non-invasively image 3-D root systems architecture
901 in soil. Plant and Soil **352:** 1-22
902 **Oburger E, Schmidt H** (2016) New Methods To Unravel Rhizosphere Processes.
903 Trends Plant Sci **21:** 243-255
904 **Oldroyd GE, Murray JD, Poole PS, Downie JA** (2011) The rules of engagement in
905 the legume-rhizobial symbiosis. Annu Rev Genet **45:** 119-144
906 **Philippot L, Raaijmakers JM, Lemanceau P, van der Putten WH** (2013) Going
907 back to the roots: the microbial ecology of the rhizosphere. Nat Rev Microbiol
908 **11:** 789-799
909 **Pini F, Galardini M, Bazzicalupo M, Mengoni A** (2011) Plant-bacteria association
910 and symbiosis: are there common genomic traits in alphaproteobacteria? Genes
911 (Basel) **2:** 1017-1032
912 **Poole P, Allaway D** (2000) Carbon and nitrogen metabolism in Rhizobium. Adv
913 Microb Physiol **43:** 117-163
914 **Poole PS, Schofield NA, Reid CJ, Drew EM, Walshaw DL** (1994) Identification of
915 chromosomal genes located downstream of dctD that affect the requirement for
916 calcium and the lipopolysaccharide layer of Rhizobium leguminosarum.
917 Microbiology **140 (Pt 10):** 2797-2809
918 **Ramachandran VK, East AK, Karunakaran R, Downie JA, Poole PS** (2011)
919 Adaptation of Rhizobium leguminosarum to pea, alfalfa and sugar beet
920 rhizospheres investigated by comparative transcriptomics. Genome Biol **12:**
921 R106
922 **Sambrook J, Fritsch EF, Maniatis T** (1989) Molecular cloning : a laboratory manual,
923 Ed 2nd. Cold Spring Harbor Laboratory, Cold Spring Harbor, N.Y.
924 **Schloter M, Wiehe W, Assmus B, Steindl H, Becke H, Hoflich G, Hartmann A**
925 (1997) Root colonization of different plants by plant-growth-promoting

926 Rhizobium leguminosarum bv. trifolii R39 studied with monospecific
927 polyclonal antisera. Appl Environ Microbiol **63:** 2038-2046
928 **Somasegaran P, Hoben HJ** (1994) Handbook for Rhizobia: Methods in Legume-
929 Rhizobium Technology. Springer-Verlag, New York
930 **Sørensen J, Haubjerg Nicolaisen M, Ron E, Simonet P** (2009) Molecular tools in
931 rhizosphere microbiology—from single-cell to whole-community analysis.
932 Plant and Soil **321:** 483-512
933 **Tecon R, van der Meer JR** (2006) Information from single-cell bacterial biosensors:
934 what is it good for? Curr Opin Biotechnol **17:** 4-10
935 **Terpolilli JJ, Hood GA, Poole PS** (2012) What determines the efficiency of N_2-
936 fixing Rhizobium-legume symbioses? Adv Microb Physiol **60:** 325-389
937 **Terpolilli JJ, Masakapalli SK, Karunakaran R, Webb IU, Green R, Watmough**
938 **NJ, Kruger NJ, Ratcliffe RG, Poole PS** (2016) Lipogenesis and Redox
939 Balance in Nitrogen-Fixing Pea Bacteroids. J Bacteriol **198:** 2864-2875
940 **Tett AJ, Karunakaran R, Poole PS** (2014) Characterisation of SalRAB a salicylic
941 acid inducible positively regulated efflux system of Rhizobium leguminosarum
942 bv viciae 3841. PLoS One **9:** e103647
943 **Tomek J, Novak O, Syka J** (2013) Two-Photon Processor and SeNeCA: a freely
944 available software package to process data from two-photon calcium imaging
945 at speeds down to several milliseconds per frame. J Neurophysiol **110:** 243-256
946 **Turner TR, James EK, Poole PS** (2013a) The plant microbiome. Genome Biol 14:
947 209
948 **Turner TR, Ramakrishnan K, Walshaw J, Heavens D, Alston M, Swarbreck D,**
949 **Osbourn A, Grant A, Poole PS** (2013b) Comparative metatranscriptomics
950 reveals kingdom level changes in the rhizosphere microbiome of plants. ISME
951 J **7:** 2248-2258
952 **Udvardi M, Poole PS** (2013) Transport and metabolism in legume-rhizobia symbioses.
953 Annu Rev Plant Biol **64:** 781-805
954 **Yagi K** (2007) Applications of whole-cell bacterial sensors in biotechnology and
955 environmental science. Appl Microbiol Biotechnol **73:** 1251-1258
956 **Ye H, Gemperline E, Venkateshwaran M, Chen R, Delaux P-M, Howes-Podill M,**
957 **Ane J-M, Li L** (2013) MALDI mass spectrometry-assisted molecular imaging

of metabolites during nitrogen fixation in the *Medicago truncatula-Sinorhizobium meliloti* symbiosis. The Plant Journal **75:** 130-145

Yobi A, Wone BWM, Xu W, Alexander DC, Guo L, Ryals JA, Oliver M, Cushman JC (2012) Comparative metabolic profiling between desiccation-sensitive and desiccation-tolerant species of Selaginella reveals insights into the resurrection trait. The Plant Journal **72**: 983-99

Figure Legends

Figure 1. *In vivo* spatial and temporal mapping images of pea root colonization and nodulation with wild-type Rlv3841 luminescently-labelled with a constitutive neomycin phophotransferase promoter controlling Lux expression in pIJ11282 (Frederix et al., 2014). A, Images were acquired at 4, 8, 11, 15, 18 and 22 dpi, with nodules visible to the naked eye at between 11 and 15 dpi (scale: 300-12,000 cps). B, Mean luminescence (pxl mm^{-2}) with standard errors shown by bars.

Figure 2. *In vivo* spatial and temporal mapping images of pea roots with biosensors detecting: sucrose (A) (scale: 200-65,535 cps), *myo*-inositol (B) (scale: 150-5,000 cps), malonate (C) (scale: 50-2,000 cps), and phenylalanine (D) (scale: 150-15,000 cps). Images were acquired at 4, 8, 11, 15, 18 and 22 dpi, with nodules visible to the naked eye between 11 and 15 dpi. These images are representative of those from biosensors in wild-type Rlv3841 background which nodulates peas.

Comparison of mean luminescence intensity *per* pixel from pea roots inoculated with biosensors in wild-type Rlv3841 background (dark gray) and Rlv3841 *nodC128*::Tn*5* background (light gray). Only wild-type Rlv3841 can form nodules. The biosensors detect: sucrose (E), *myo*-inositol (F), malonate (G) and phenylalanine (H). Standard errors are shown by bars, stars indicate significant differences between a biosensor in wild-type Rlv3841 and Rlv3841 *nodC128*::Tn*5* backgrounds (t-test, * = $p < 0.05$; ** = $p < 0.01$). Differences between each time point (ANOVA with post hoc Tukey test, $p < 0.05$) are reported in Supplemental Tables S4 and S5. For representative images from Rlv3841 *nodC128*::Tn*5* background see Supplemental Fig. S8.

Close-up light-field photograph and luminescence of roots showing nodules at 15 dpi inoculated with biosensors detecting: sucrose (I), *myo*-inositol (J), malonate (K), and phenylalanine (L).

Figure 3. Comparison of mean luminescence intensity *per* pixel from pea roots inoculated with biosensors in wild-type Rlv3841 (dark gray) or the Rlv3841 *nodC128*::Tn*5* mutant (light gray). Only wild-type Rlv3841 can form nodules. Biosensors detect: xylose (A), fructose (B), C4-dicarboxylates (C) tartrate (D), GABA (E) and hesperetin (F). Standard errors are shown by bars, stars indicate significant differences between a biosensor in wild-type Rlv3841 and Rlv3841 *nodC128*::Tn*5* (t-

test, * = p <0.05; ** = p <0.01). Differences between each time point (ANOVA with post hoc Tukey test, p<0.05) are reported in Supplemental Tables S4 and S5. For representative images from Rlv3841 and Rlv3841 *nodC128*::Tn*5* background see Supplemental Figs. S5 and S9, respectively.

Figure 4. Comparison of mean luminescence (cps mm^{-2}) from pea nodules of different ages with biosensors in wild-type Rlv3841 (dark gray) or Rlv3841 *nifH*::ΩSp mutant (white) background. Nodules formed by Rlv3841 fix nitrogen whereas those formed by these mutant strains are unable to do so. Biosensors are specific for: constitutively active (A), sucrose (B), *myo*-inositol (C), C4-dicarboxylates (D) and GABA (E). Standard errors are shown by bars and stars indicate significant differences between a biosensor in wild-type Rlv3841 and the Rlv3841 *nifH*::ΩSp mutant (t-test, * = p <0.05; ** = p <0.01). Differences between each time point (ANOVA with post hoc Tukey test, p <0.05) are reported in Supplemental Tables S6 and S7.

Figure 5. Comparison of mean luminescence (cps mm^{-2}) from vetch roots inoculated with biosensors in wild-type Rlv3841 background. Biosensors detect: xylose (A), fructose (B), sucrose (C), *myo*-inositol (D), malonate (E), C4-dicarboxylates (F), phenylalanine (G), GABA (H) and hesperetin (I). Standard errors are shown by bars. Differences between each time point (ANOVA with post hoc Tukey test, p <0.05) are reported in Supplemental Table S8. Nodules are visible to the naked eye from 8 dpi.

Figure 6. Time-course of hesperetin detection on a vetch seedling root from 1 to 22 dpi. Arrows indicate spots where luminescence is concentrated and a nodule forms later.

Figure 7. Summary of metabolite detection on pea roots; in the rhizosphere (≤11 dpi) and within nitrogen-fixing nodules (≥15 dpi). Lines on the left-hand side group similar chemicals into; sugars and polyols, organic acids, amino acids, and flavonoids. Color shows level detected in rhizosphere and nodules: high, red; medium, dark pink; low, pale pink; barely detected, gray; not detected, black.

Supplemental Data

The following supplemental data are available

Supplemental Figure S1. Workflow of the NightCROP image processing script, the picture is a pea inoculated with a constitutively expressed bioreporter at 15 dpi. A, NightOWL output photographic image of the pea root system. B, NightOWL output luminescent image of same area captured in A. C, NightOWL superimposed image of pictures A and B with false colors. D, NightCROP segmentation of picture A, the program detects difference in light intensity and draws a segmentation mask over the root system. E, Segmentation mask is applied on picture B and luminescence intensity is specifically extracted from the segmented area (pxl/mm^2). F, Mean background luminescence is calculated around each segmented pixel and, subtracting this from the intensity value of the pixel.

Supplemental Figure S2. *In vivo* spatial and temporal mapping images of pea root colonization and nodulation with wild-type Rlv3841 luminescently-labelled with a constitutive neomycin phophotransferase promoter controlling Lux expression in pIJ11282 (Frederix et al., 2014). Images were acquired at 4, 8, 11, 15, 18 and 22 dpi, with nodules visible to the naked eye at between 11 and 15 dpi (scale: 50-12,000 cps).

Supplemental Figure S3. Luminescence is not detected in the absence of plant roots. Luminescence of biosensors on FP media supplemented with pyruvate and ammonium chloride after 7 days' growth (scale: 50-1,000 cps).

Supplemental Figure S4. *In vivo* spatial and temporal mapping images of pea roots inoculated with the xylose biosensor, flooded with xylose at 4 dpi (A); the sucrose biosensor, flooded with sucrose at 4 dpi (B); the GABA biosensor, flooded with GABA at 4 dpi (C); the sucrose biosensor, flooded with GABA at 4 dpi (D) and the GABA biosensor, flooded with sucrose at 4 dpi (E) (scale: 500-5,000 cps). For each, images were taken before, and 5 min, 3 hr, and 21 hr post-flooding.

Supplemental Figure S5. *In vivo* spatial and temporal mapping images of pea roots with biosensors detecting: sugars, xylose (A) (scale: 400-12,000 cps) and fructose (B)

(scale: 300-12,000 cps), organic acids, C4-dicarboxylates (C) (scale: 400-65,535 cps) and tartrate (D) (scale: 200-15,000 cps), amino acid, GABA (E) (scale: 500-10,000 cps) and flavonoid, hesperetin (F) (scale: 250-13,000 cps). Images were acquired at 4, 8, 11, 15, 18 and 22 dpi with nodules visible to the naked eye at between 11 and 15 dpi. These images are representative of those from biosensors in wild-type Rlv3841 background.

Supplemental Figure S6. Comparison of pea roots inoculated with biosensors in wild-type Rlv3841 and Rlv3841 *nodC128*::Tn*5* mutant background. Only wild-type Rlv3841 strains are able to form nodules. Biosensors detect: polyols, erythritol (A, E and I) (scale: 100-1,000) and mannitol (B, F and J) (scale: 50-700), the organic acids, formate (C, G and K) (scale: 100-2,000) and salicylic acid (D, H and L) (scale: 100-2,000). A-D, Images representative of biosensors in Rlv3841 background. E-H, Comparison of mean luminescence (pxl mm^{-2}) from pea roots inoculated with biosensors in wild-type Rlv3841 background (dark gray) and Rlv3841 *nodC128*::Tn*5* background (light gray). Standard errors are shown by bars. I-L, Images representative of biosensors in Rlv3841 *nodC128*::Tn*5* mutant background.

Supplemental Figure S7. Comparison of mean luminescence (cps mm^{-2}) of pea nodules from 15 to 22 dpi, with biosensors in wild-type Rlv3841 background. Biosensors are specific for: xylose (A), fructose (B), phenylalanine (C) and hesperetin (D). Standard errors are shown by bars.

Supplemental Figure S8. *In vivo* spatial and temporal mapping images of pea roots with biosensors detecting: sucrose (A) (scale: 200-65,535 cps), *myo*-inositol (B) (scale: 50-2,000 cps), malonate (C) (scale: 50-2,000 cps) and phenylalanine (D) (scale: 150-15,000 cps). Images were acquired at 4, 8, 11, 15, 18 and 22 dpi. These images are representative of those from biosensors in Rlv3841 *nodC128*::Tn*5* background and are unable to nodulate peas.

Supplemental Figure S9. *In vivo* spatial and temporal mapping images of pea roots with biosensors detecting: sugars, xylose (A) (scale: 400-12,000 cps) and fructose (B) (scale: 300-12,000 cps), organic acids, C4-dicarboxylates (C) (scale: 400-65,535 cps) and tartrate (D) (scale: 200-15,000), amino acid, GABA (E) (scale: 500-10,000 cps) and flavonoid, hesperetin (F) (scale: 250-13,000 cps). Images were acquired at 4, 8, 11,

15, 18 and 22 dpi. These images are representative of those from biosensors in Rlv3841 *nodC128*::Tn*5* background and are unable to nodulate peas.

Supplemental Figure S10. Comparison of mean luminescence (cps mm^{-2}) from pea roots inoculated with biosensors in wild-type Rlv3841 background (dark gray) and Rlv3841 *nifH*::ΩSp mutant background (white). Values for *nifH*::ΩSp mutant are adjusted for the lower level of constitutive Lux expression in this background (Fig. 4) to show equivalent expression in a wild-type background. Only wild-type Rlv3841 strains are able to form nitrogen-fixing nodules. Biosensors detect: sucrose (A), *myo*-inositol (B), C4-dicarboxylates (C), and GABA (D). Standard errors are shown by bars and stars indicate significant differences between a biosensor in wild-type Rlv3841 and Rlv3841 *nifH*::ΩSp mutant background (t-test, * = $p < 0.05$; ** = $p < 0.01$).

Supplemental Figure S11. Investigation of the role of malonate during root attachment. A, Whole root attachment assay showing the number of bacteria attached after 1 h incubation for wild-type Rlv3841[pIJ11282], Rlv3841 *matC*::pK19 [pIJ11282] and Rlv3841 *matA*::pK19[pIJ11282], mutated in malonate transport and catabolism respectively. Plasmid pIJ11282 has constitutively expressed *lux* genes (Frederix et al., 2014). Standard errors are shown by bars. Different letters are used to indicate significant difference (ANOVA with post hoc HSD Tukey test, $p < 0.05$) between groups. B, Competition test on pea plants at 7 dpi. Histograms represent luminescence/area of constitutive reporter pIJ11282. Strains Rlv3841[pIJ11282] or Rlv3841 *matC*::pK19 [pIJ11282] were inoculated in ratio 1:1 with Rlv3841 or Rlv3841 *matC*::pK19. Standard errors are shown by bars.

Supplemental Table S1. Strains and plasmids used in this work. St (streptomycin), Neo (neomycin), Tc (tetracycline) and Sp (spectinomycin).

Supplemental Table S2. Conditions used to test specificity the bioreporter library.

Supplemental Table S3. Metabolomic data from root exudates of *P. sativum.*

Supplemental Table S4. ANOVAs with post hoc Tukey test ($p < 0.05$) on total luminescence for bioreporters in Rlv3841 inoculated onto pea plants (Fig. 2 and 3).

Supplemental Table S5. ANOVAs with post hoc Tukey test ($p < 0.05$) on total luminescence for bioreporters in Rlv3841 *nodC128*::Tn*5* inoculated onto pea plants (Fig. 2 and 3).

Supplemental Table S6. ANOVAs with post hoc Tukey test ($p < 0.05$) on nodules luminescence for bioreporters in Rlv3841 inoculated onto pea plants (Fig. 4).

Supplemental Table S7. ANOVAs with post hoc Tukey test ($p < 0.05$) on nodules luminescence for bioreporters in Rlv3841 *nifH*::ΩSp inoculated onto pea plants (Fig. 4).

Supplemental Table S8. ANOVAs with post hoc Tukey test ($p < 0.05$) on total luminescence for bioreporters in Rlv3841 inoculated onto vetch plants (Fig. 5).

Supplemental Table S9. Primers used in this work.

Supplemental Table S10. Relative expression in microarray experiments under seventy-three different conditions of the *R. leguminosarum* genes whose promoters were used for construction of biosensors.

1152 **Table I.** *Characterization of biosensors from R. leguminosarum*
1153

Biosensor	Inducer(s)	Fold-induction	Sensitivity (mM)	Specific luminescence (RLU/OD_{600})	Gene	Name	Function of protein encoded by gene
Sugars and polyols							
Xylose	Xylose	7.20 (±0.34)	1	1.10×10^7	RL2720[b]	*rbsC*	Transport, permease of ABC, CUT2
	Lyxose	6.99 (±0.37)		1.12×10^7			
Fructose	Fructose	16.13 (±1.07)	0.01	2.84×10^7	RL0489[c]	*frcB*	Transport, SBP of ABC, CUT2
	Lactulose	11.10 (±0.87)		1.97×10^7			
	Mannitol	8.94 (±0.26)		1.51×10^7			
	Mannose	8.41 (±0.46)		1.47×10^7			
	Sorbitol	8.94 (±0.58)		1.61×10^7			
	Sucrose	7.00 (±0.21)		1.18×10^7			
Sucrose	Sucrose	36.35 (±1.77)	0.1	2.94×10^7	pRL120556[c]		Transport, SBP of ABC, CUT1
	Raffinose	34.19 (±4.43)		2.93×10^7			
Erythritol	Erythritol	4.72 (±0.50)	1	2.47×10^5	pRL90085[b]		Transport, SBP of ABC, CUT2
Mannitol	Mannitol	1.71×10^6 ($\pm 1.50 \times 10^6$)	0.001	5.51×10^{12}	RL4218[b]		Transport, solute binding protein (SBP) of ABC, CUT1
	Sorbitol[a]	28.52 (±3.53)		3.45×10^7			
	Adonitol[a]	13.01 (±2.39)		1.45×10^7			
***myo*-Inositol**	*myo*-Inositol	216.84 (±13.80)	0.1	4.00×10^7	RL4655[b,c]	*intA*	Transport, SBP of ABC, CUT2
Organic acids							
Formate	Formate	27.20 (±2.13)	10	2.02×10^6	RL4393[b]	*fdsG*	Metabolism, formate dehydrogenase
Malonate	Malonate	540.48 (±155.87)	10	5.69×10^6	RL0990[b]	*matA*	Metabolism
C4-dicarboxylates	Succinate	87.83 (±3.46)	0.1	2.28×10^7	RL3424[b]	*dctA*	Transport, dicarboxylate transporter
	Malate	57.19 (±9.18)	0.01	2.86×10^7			

	Aspartate	33.18 (±3.02)	10	1.28 x 10^7			
Tartrate	Tartrate	188.68 (±10.51)	0.1	2.32 x 10^7	RL0996[b]		Transport, permease of MFS uptake system
Salicylic acid	Salicylic acid	1024.87 (±161.97)	1	1.78 x 10^7	RL1329	*salA*	Transport, MFS efflux system
Amino acids							
Phenylalanine	Phenylalanine	52.10 (±8.43)	0.01	4.08 x 10^7	RL1860[b]	*phhA*	Metabolism, phenylalanine-4-hydroxylase
GABA	GABA	3.56 (±1.28)	0.5	5.34 x 10^4	RL0102[d]	*gabT*	Metabolism, 4-aminobutyrate aminotransferase
Flavonoids							
Hesperetin	Hesperetin	256.44 (±68.68)	0.001	1.63 x 10^7	pRL100185[b,c]	*nodABC*	Metabolism, Nod factor synthesis

Abbreviations used: RLU (relative luminescence units), ABC (ATP binding cassette transporter); CUT1, CUT2 (carbohydrate uptake transporter-1 and -2); SBP (substrate binding protein); MFS (major facilitator superfamily). Inducer(s) are solute(s) that give the highest fold-induction and specific luminescence. Biosensor induction by a solute is described as specific if the specific luminescence is ≥10-fold that observed from the other solutes tested. The biosensors for erythritol, formate, and GABA have a relatively high expression with a variety of non-related solutes (background) and they are described as being specific for these solutes, respectively, with specific luminescence ≥4-fold values obtained with other solutes. More than one compound is considered inducing when the fold-induction is > 40% of the maximum fold-induction for a biosensor. Fold-induction is the ratio of RLU/OD_{600} when grown in the presence of solute (Supplemental Table S2 gives solute concentration), to RLU/OD_{600} when grown in absence of solute. Sensitivity is the minimum concentration of substrate spotted onto bacteria growing in agar to give a luminescent signal visible with a NightOWL camera after 4 h incubation. [a] Fold-induction is <40% that of the best inducer and therefore not considered to be specific induction. [b] indicates genes induced >3-fold, $p \leq 0.05$ in the pea rhizosphere (Ramachandran et al. 2011). [c] indicates genes induced >3-fold, $p \leq 0.05$ by pea exudate (Ramachandran et al. 2011). [d] indicates genes induced >3-fold, $p \leq 0.05$ in the alfalfa rhizosphere (Ramachandran et al. 2011).

Table II. *Results from microarrays comparing the effect of pea root exudate and the pea rhizosphere on expression of genes used to develop biosensors*

Biosensor	Gene	Fold-expression with added 23 d-old pea root exudate [a,b]	Fold-expression in 21 d-old pea rhizosphere [b,c]
Sugars and polyols			
Xylose	RL2720	1.21†	4.00
Fructose	RL0489	18.52	1.65
Sucrose	pRL120556	3.31	1.03†
Erythritol	pRL90085	1.34†	5.74
Mannitol	RL4218	4.30†	3.18
***myo*-Inositol**	RL4655	26.94	2.71
Organic acids			
Formate[d]	RL4393	0.88†	7.52
Malonate	RL0992	1.48†	1.31†
C4-dicarboxylates	RL3424	0.67†	23.00
Tartrate	RL0996	3.34†	5.70
Salicylic acid[d]	RL1329	1.18†	2.27
Amino acids			
Phenylalanine	RL1860	0.86†	46.28
GABA	RL0102	2.90	1.14†
Flavonoids			
Hesperetin[d]	pRL100185	49.15	2.09

[a] Microarrays performed in triplicate on free-living Rlv3841cells grown with and without the addition of pea root exudate (part of the sample used for metabolomic analysis). [b] $p \leq 0.05$, unless marked † when $p > 0.05$; fold-expression >1 are an increase in expression under the condition tested. [c] Microarrays performed in triplicate on Rlv3841 extracted from rhizosphere compared with free-living cells grown in glucose/ammonia (Ramachandran et al., 2011). [d] Compound not found in metabolomic analysis of pea root exudate.

Table III. *Summary of compounds detected by biosensors in the pea rhizosphere and within nodules of Rlv3841*

Compound	Rhizosphere 4-11 dpi	Location on roots	Nodules 11-22 dpi	Nodule age at which detection peaks (dpi)
Sugars and polyols				
Xylose	Yes	Primary and lateral root tips	Yes	15-18
Fructose	Yes	Primary and lateral root tips	Yes	15-22
Sucrose	No		Yes	15-18
Erythritol[a]	No		No	
Mannitol[a]	No		No	
myo-Inositol	Yes	Primary root and lateral root tips	Yes	15-18
Organic acids				
Formate[a,b]	No		No	
Malonate	Yes	Uppermost portion of primary root and lateral roots, just before root tips	Low	15
C4-dicarboxylates	Yes	No clear pattern	Yes	15-18
Tartrate	Yes	Uppermost portion of primary root only	Low	15
Salicylic acid[a,b]	No		No	
Amino acids				
Phenylalanine	Yes	Root elongation zone of lateral roots	Yes	15
GABA	No		Yes	15-18
Flavonoids				
Hesperetin[b]	Yes	Lateral roots	Yes	15

[a] Luminescence from biosensor detecting this compound was very low throughout the time course examining the pea rhizosphere. [b] Compound not listed as present in metabolomics analysis of pea exudate. dpi, days post-inoculation.

Table IV. *Summary of compounds detected by biosensors in the vetch rhizosphere and within nodules of Rlv3841*

Compound	Rhizosphere 4 dpi	Nodules 8-22 dpi	Nodule age at which detection peaks (dpi)[a]
Sugars and polyols			
Xylose	Yes	Yes	22
Fructose	Yes	Yes	(8) 11 (14-22)
Sucrose	No	Yes	(8) 11 (14-22)
Erythritol[b]	No	No	
Mannitol[b]	No	No	
myo-Inositol	Yes	Yes	22
Organic acids			
Formate[b]	No	No	
Malonate	Yes	No	
C4-dicarboxylates	Yes	Yes	(8-11) 14 (18-22)
Tartrate[b]	No	No	
Salicylic acid[b]	No	No	
Amino acids			
Phenylalanine	No	Yes	(18) 22
GABA	No	Yes	8 (11-14)
Flavonoids			
Hesperetin	Yes	No	

[a] Brackets indicate when there is less than the maximum detected. [b] Luminescence from biosensor detecting this compound was very low throughout the time course examining the vetch rhizosphere. dpi, days post-inoculation.

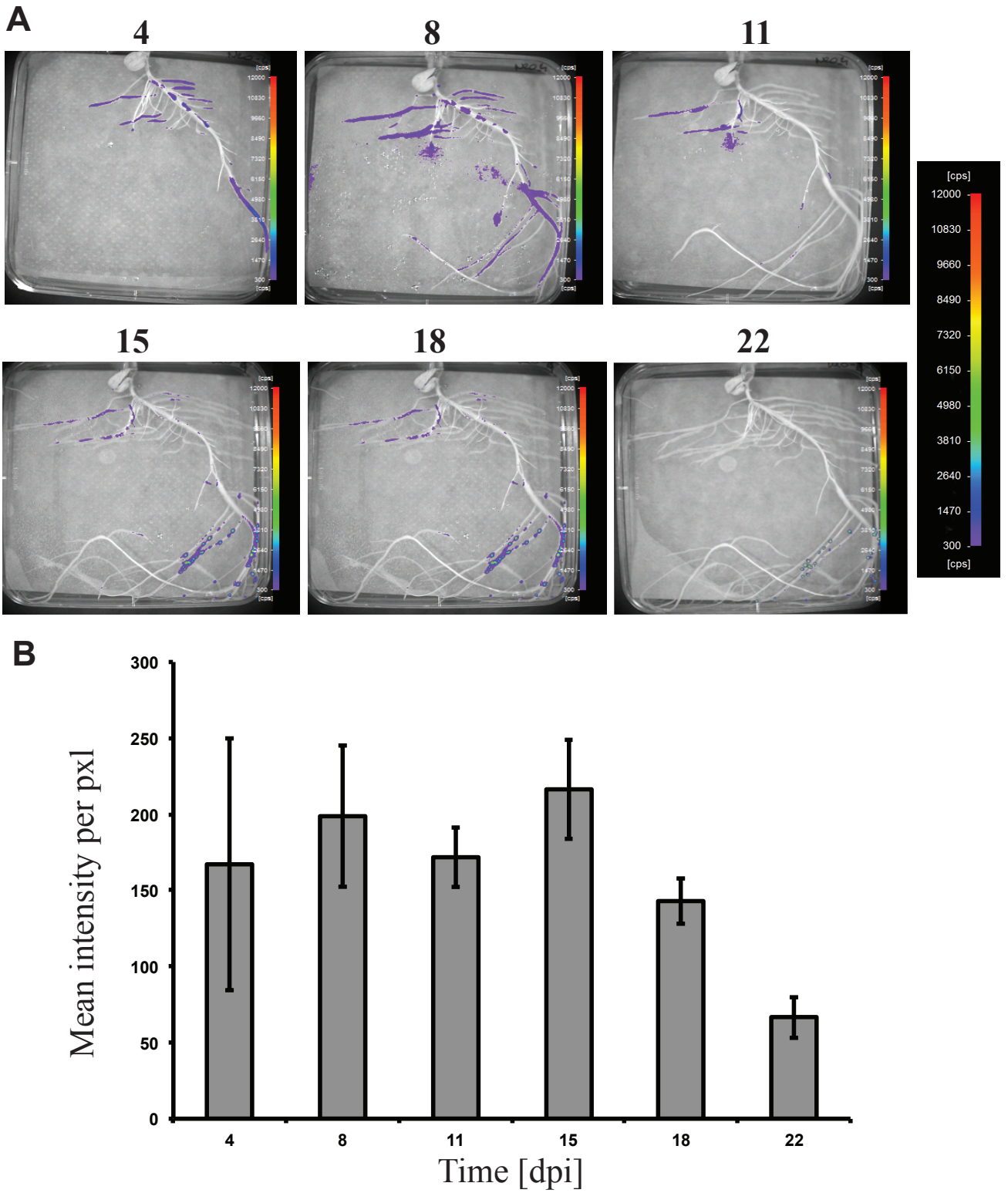

Figure 1. In vivo spatial and temporal mapping images of pea root colonization and nodulation with wild-type Rlv3841 luminescently-labelled with a constitutive neomycin phophotransferase promoter controlling Lux expression in pIJ11282 (Frederix et al., 2014). A, Images were acquired at 4, 8, 11, 15, 18 and 22 dpi, with nodules visible to the naked eye between 11 and 15 dpi. B, Mean luminescence (pxl mm^{-2}) with standard errors shown by bars.

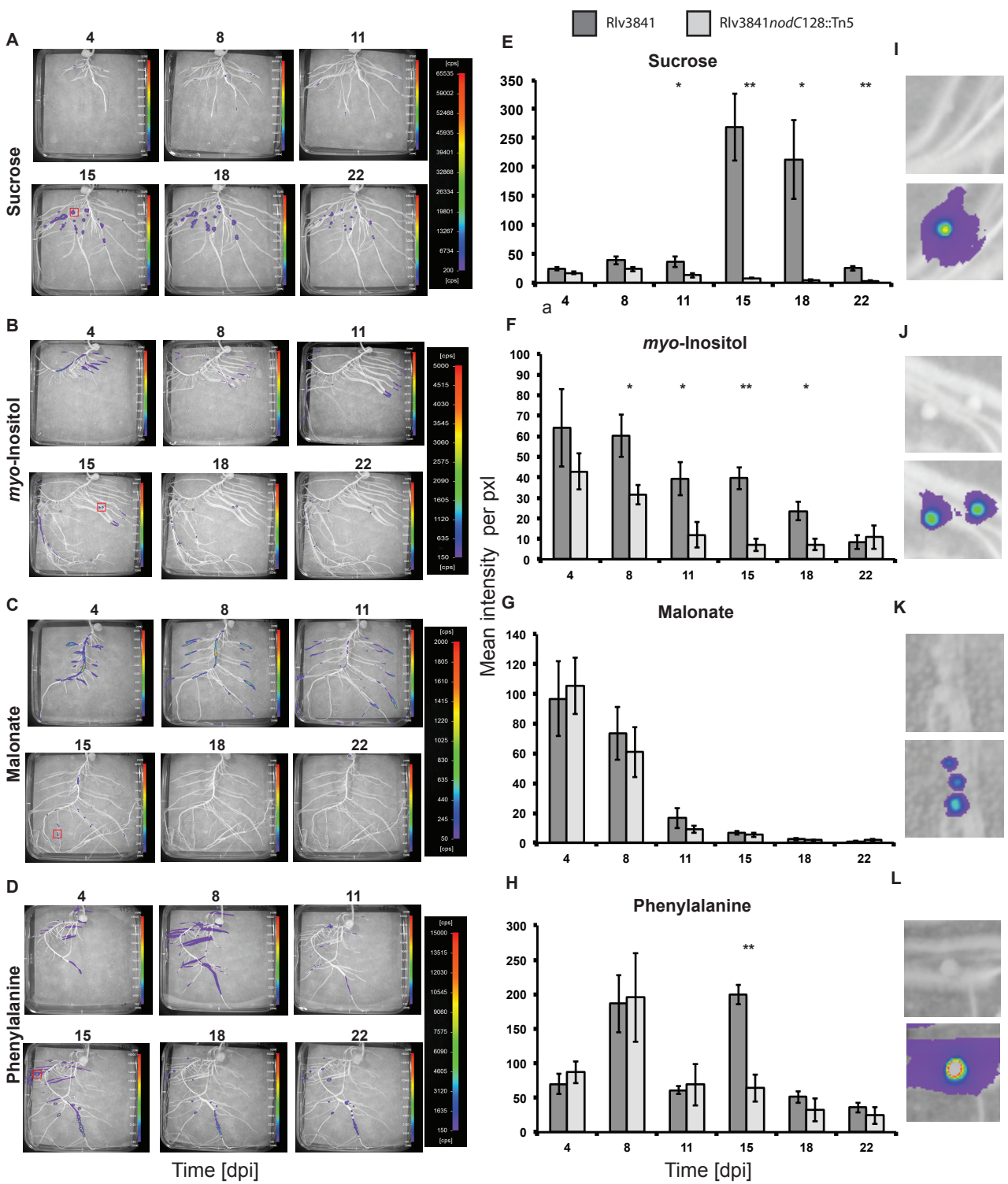

Figure 2. In vivo spatial and temporal mapping images of pea roots with biosensors detecting: sucrose (A) (scale: 200-65,535 cps), myo-inositol (B) (scale: 150-5,000 cps), malonate (C) (scale: 50-2,000 cps), and phenylalanine (D) (scale: 150-15,000 cps). Images were acquired at 4, 8, 11, 15, 18 and 22 dpi, with nodules visible to the naked eye between 11 and 15 dpi. These images are representative of those from biosensors in wild-type Rlv3841 background which nodulates peas. Comparison of mean luminescence intensity per pixel from pea roots inoculated with biosensors in wild-type Rlv3841 background (dark gray) and Rlv3841 nodC128::Tn5 background (light gray). Only wild-type Rlv3841 can form nodules. The biosensors detect: sucrose (E), myo-inositol (F), malonate (G) and phenylalanine (H). Standard errors are shown by bars, stars indicate significant differences between a biosensor in wild-type Rlv3841 and Rlv3841 nodC128::Tn5 backgrounds (t-test, * = $p < 0.05$; ** = $p < 0.01$). Differences between each time point (ANOVA with post hoc Tukey test, $p < 0.05$) are reported in Supplemental Tables S4 and S5. For representative images from Rlv3841 nodC128::Tn5 background see Supplemental Fig. S6. Close-up light-field photograph and luminescence of roots showing nodules at 15 dpi inoculated with biosensors detecting: sucrose (I), myo-inositol (J), malonate (K), and phenylalanine (L).

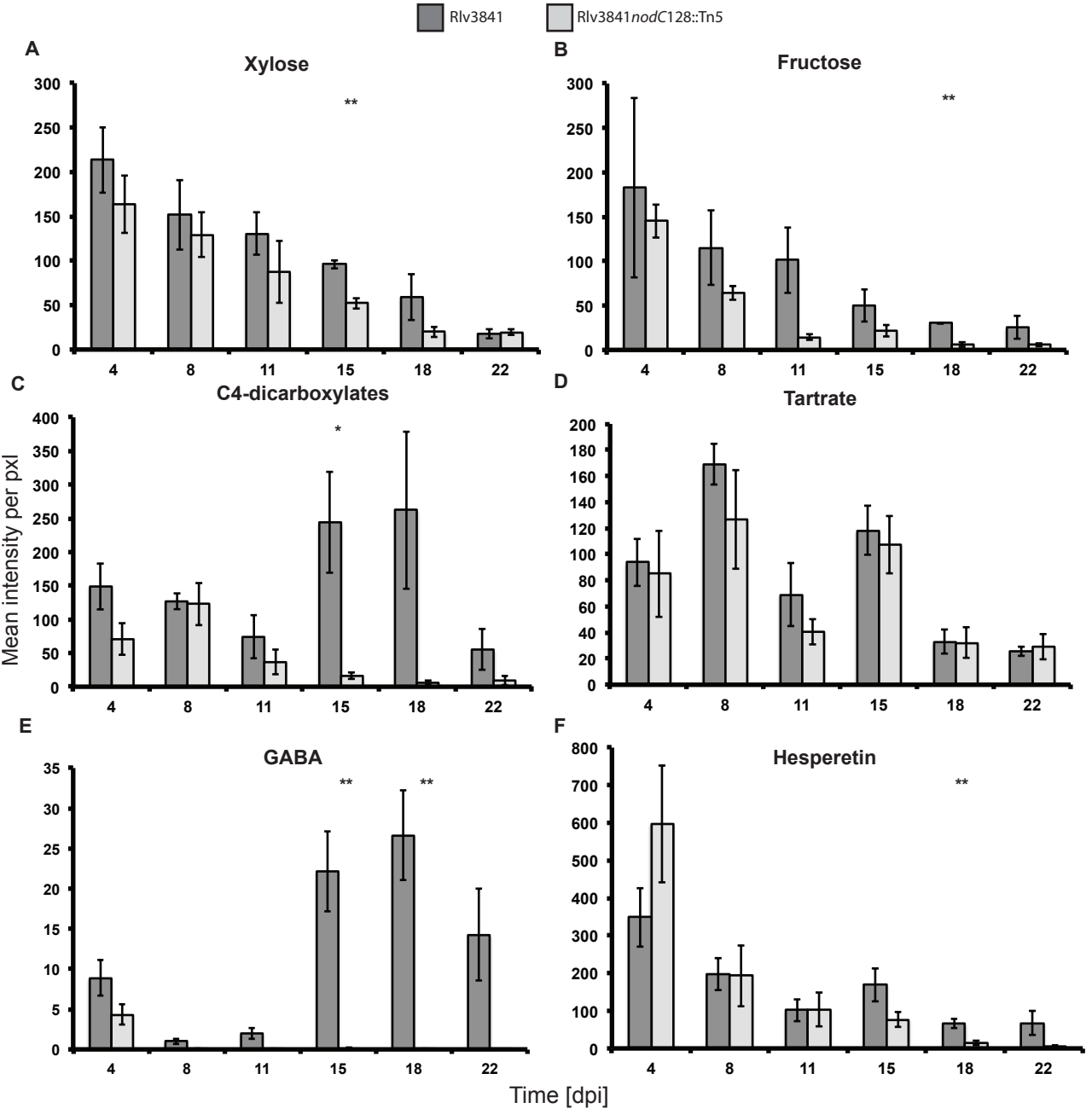

Figure 3. Comparison of mean luminescence intensity per pixel from pea roots inoculated with biosensors in wild-type Rlv3841 (dark gray) or the Rlv3841 nodC128::Tn5 mutant (light gray). Only wild-type Rlv3841 can form nodules. Biosensors detect: xylose (A), fructose (B), C4-dicarboxylates (C) tartrate (D), GABA (E) and hesperetin (F). Standard errors are shown by bars, stars indicate significant differences between a biosensor in wild-type Rlv3841 and Rlv3841 nodC128::Tn5 (t-test, * = $p < 0.05$; ** = $p < 0.01$). Differences between each time point (ANOVA with post hoc Tukey test, $p<0.05$) are reported in Supplemental Tables S4 and S5. For representative images from Rlv3841 and Rlv3841 nodC128::Tn5 background see Supplemental Figs. S6 and S7, respectively.

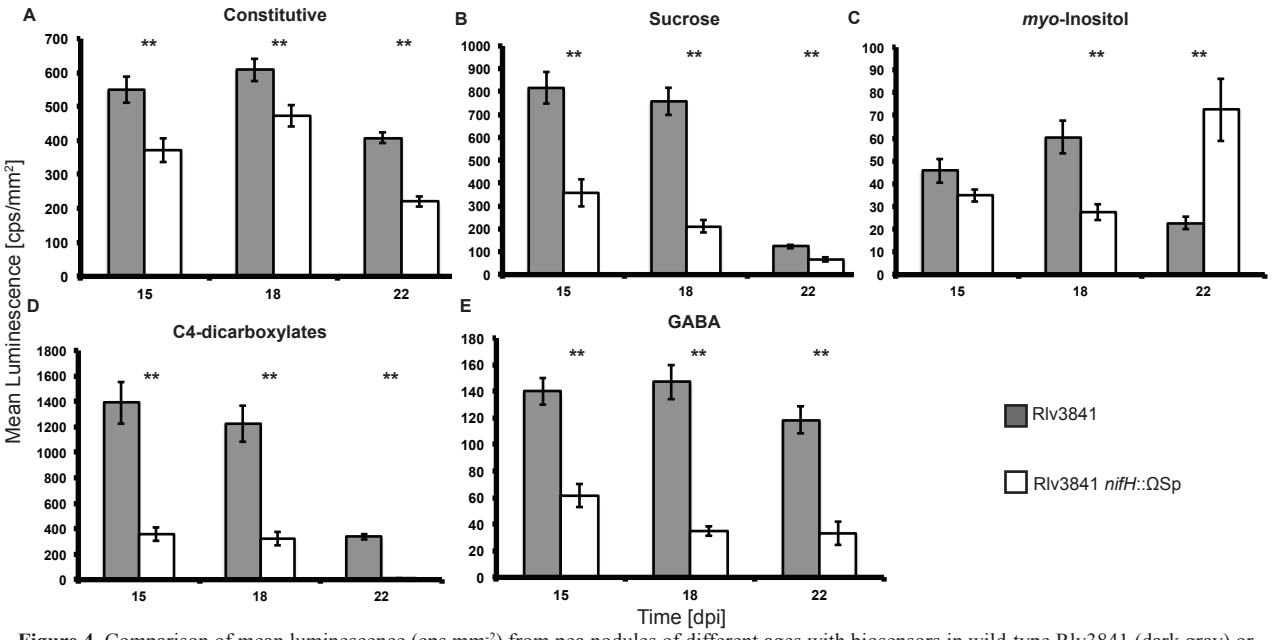

Figure 4. Comparison of mean luminescence (cps mm^{-2}) from pea nodules of different ages with biosensors in wild-type Rlv3841 (dark gray) or Rlv3841 nifH::ΩSp mutant (white) background. Nodules formed by Rlv3841 fix nitrogen whereas those formed by these mutant strains are unable to do so. Biosensors are specific for: constitutively active (A), sucrose (B), myo-inositol (C), C4-dicarboxylates (D) and GABA (E). Standard errors are shown by bars and stars indicate significant differences between a biosensor in wild-type Rlv3841 and the Rlv3841 nifH::ΩSp mutant (t-test, * = $p < 0.05$; ** = $p < 0.01$). Differences between each time point (ANOVA with post hoc Tukey test, $p < 0.05$) are reported in Supplemental Tables S6 and S7.

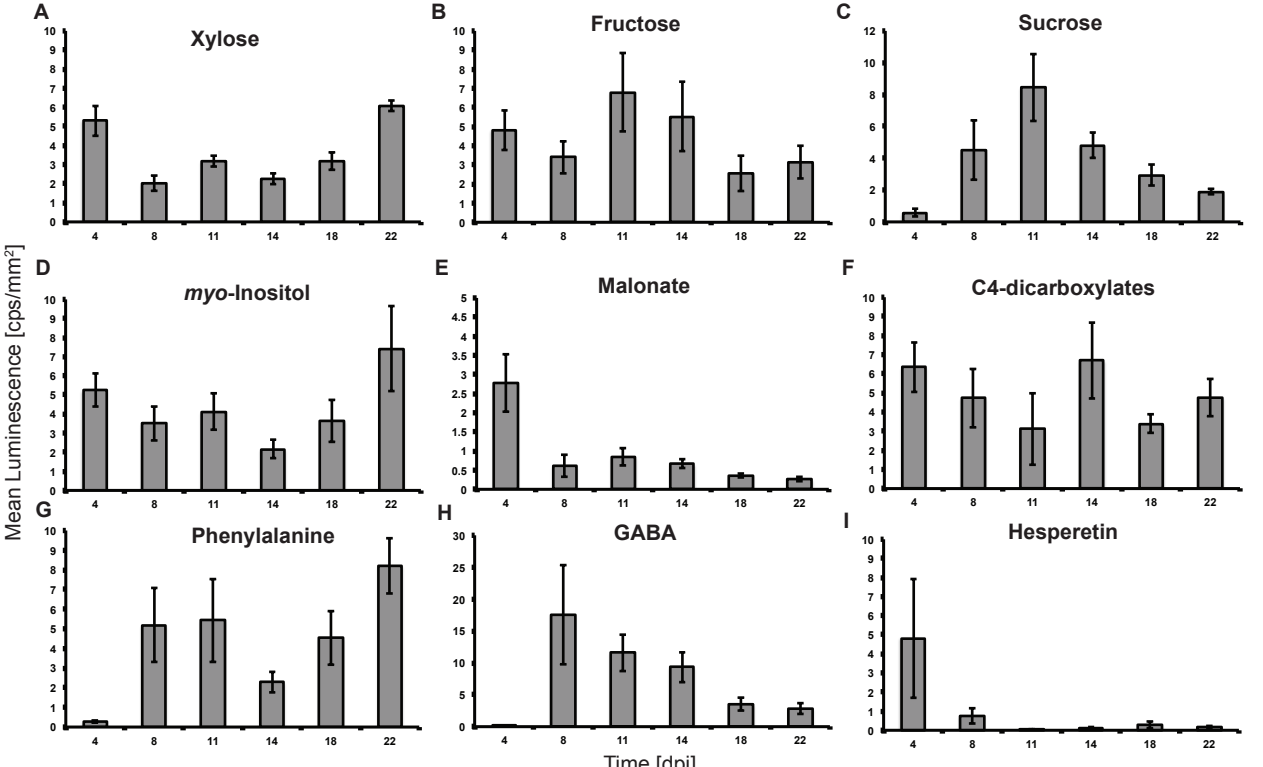

Figure 5. Comparison of mean luminescence (cps mm-2) from vetch roots inoculated with biosensors in wild-type Rlv3841 background. Biosensors detect: xylose (A), fructose (B), sucrose (C), myo-inositol (D), malonate (E), C4-dicarboxylates (F), phenylalanine (G), GABA (H) and hesperetin (I). Standard errors are shown by bars. Differences between each time point (ANOVA with post hoc Tukey test, $p < 0.05$) are reported in Supplemental Table S8. Nodules are visible to the naked eye from 8 dpi.

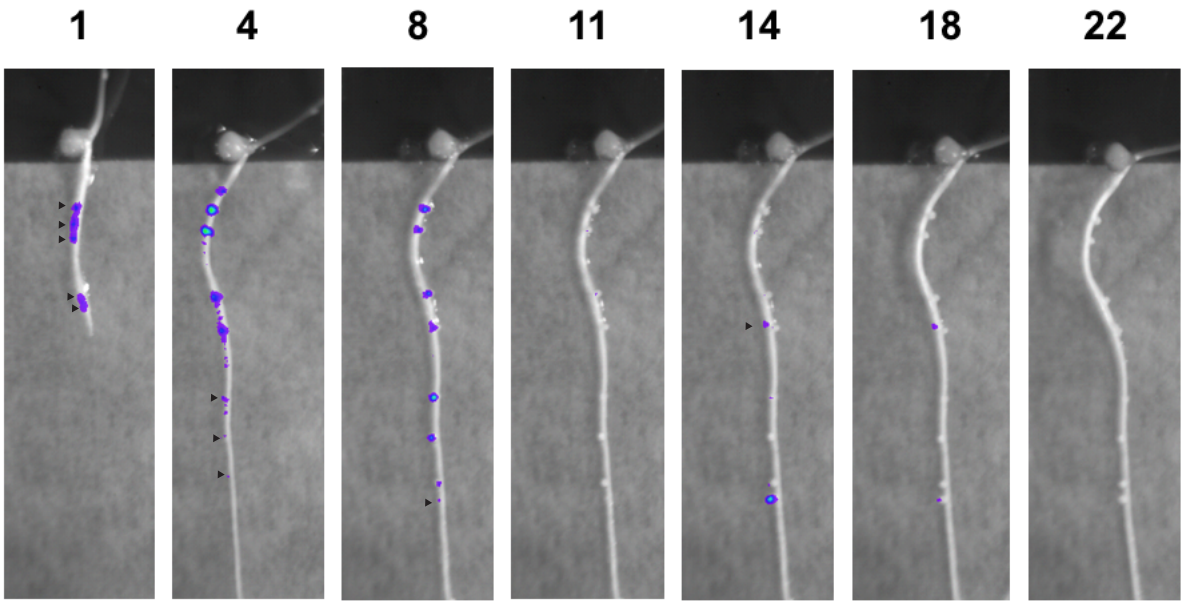

Figure 6. Time-course of hesperetin detection on a vetch seedling root from 1 to 22 dpi. Arrows indicate spots where luminescence is concentrated and a nodule forms later.

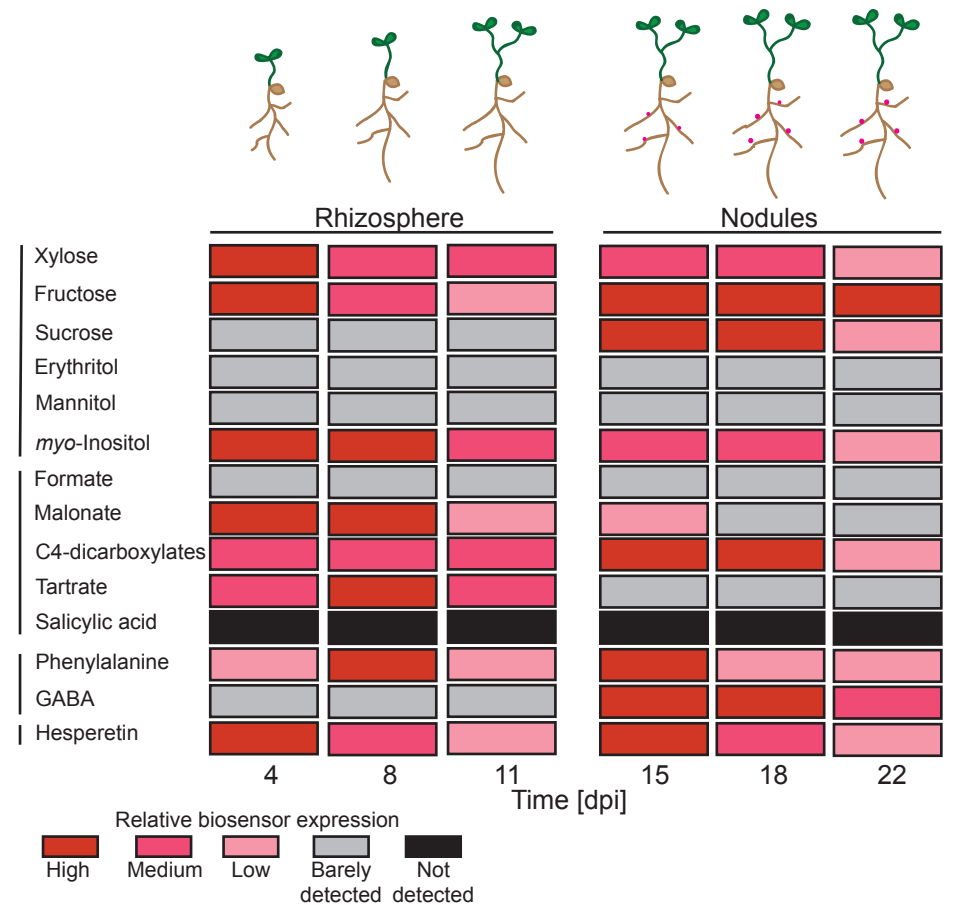

Figure 7. Summary of metabolite detection on pea roots; in the rhizosphere (≤11 dpi) and within nitrogen-fixing nodules (≥15 dpi). Lines on the left-hand side group similar chemicals into; sugars and polyols, organic acids, amino acids, and flavonoids. Color shows level detected in rhizosphere and nodules: high, red; medium, dark pink; low, pale pink; barely detected, gray; not detected, black.

NightOWL output

NightOWL reconstructed image

A Photo channel

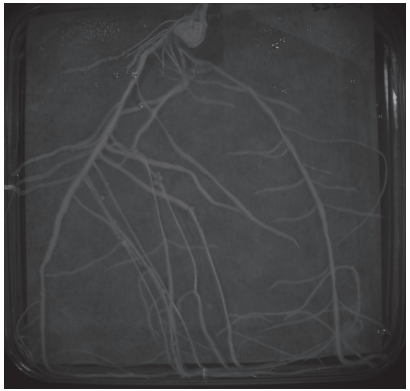

B Luminescence channel

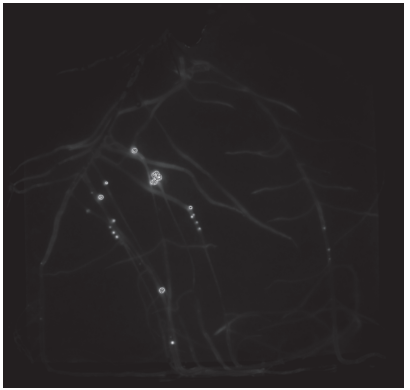

C

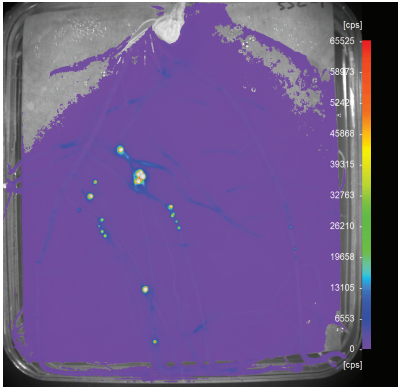

Segmentation on image of photo channel

D

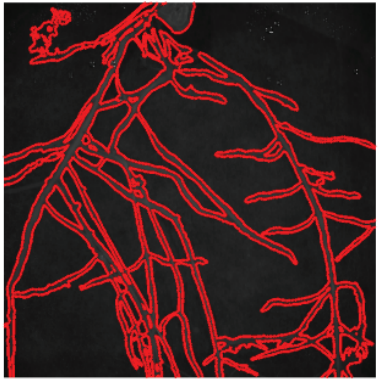

Application of the overlaid mask on the luminescence chanel

E

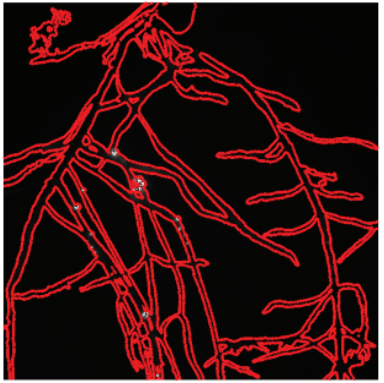

F

Extraction of the luminescence information

	1
Mean root	1.7764e+03
Median root	1032
Sum root	259486580
Median background	620
Mean root – background	1.1564e+03
Median root – background	412

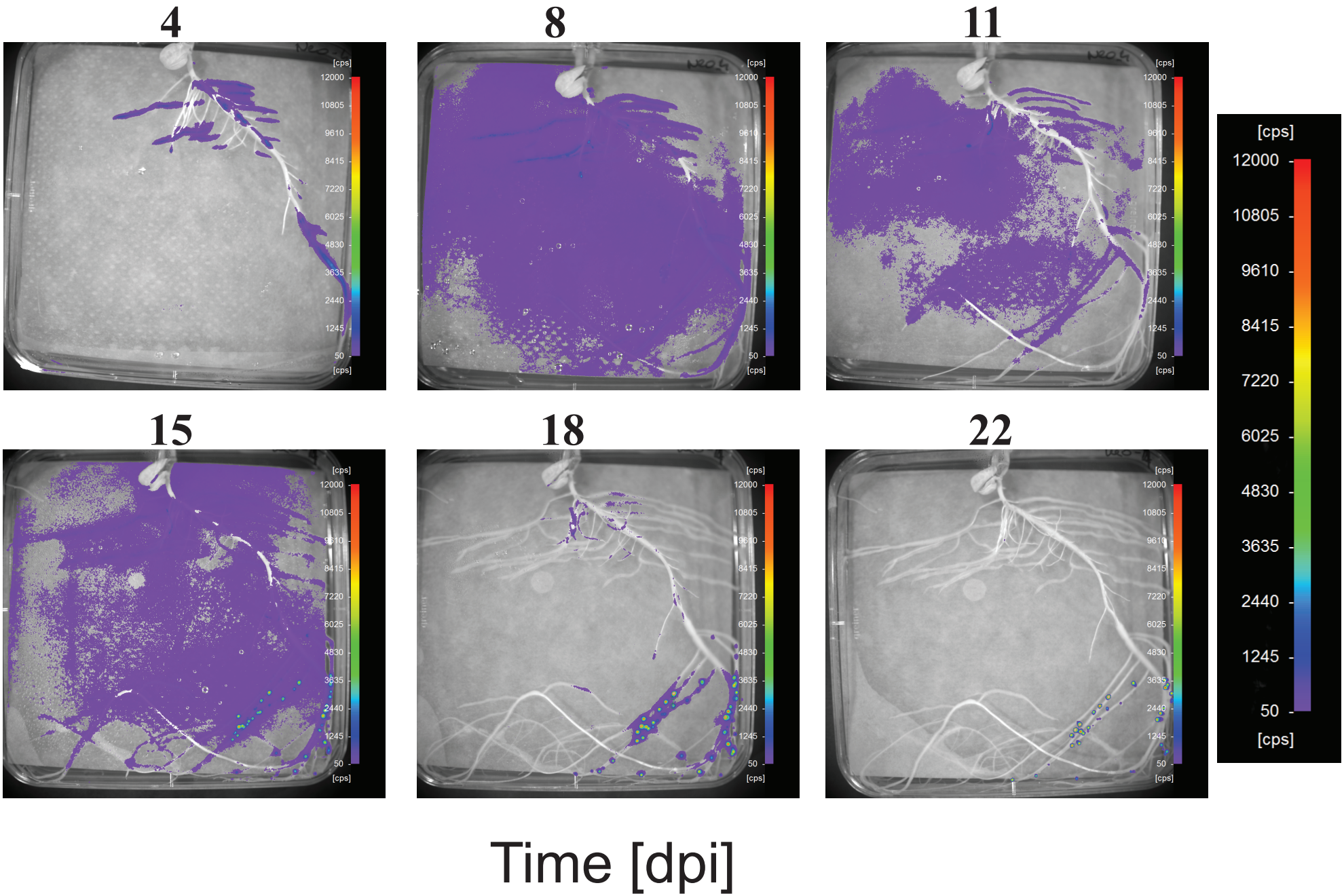
4
8
11
15
18
22
[cps]
12000
10805
9610
8415
7220
6025
4830
3635
2440
1245
50
[cps]
Time [dpi]

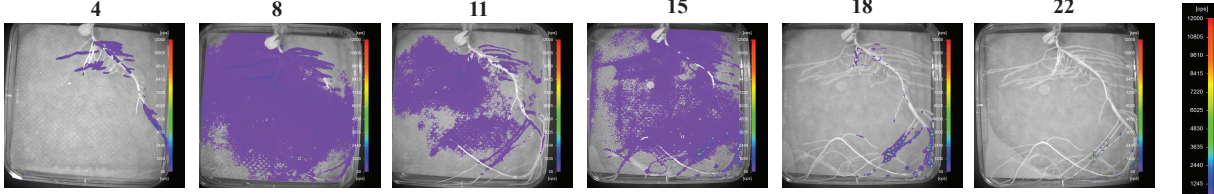
4
8
11
15
18
22
Time [dpi]

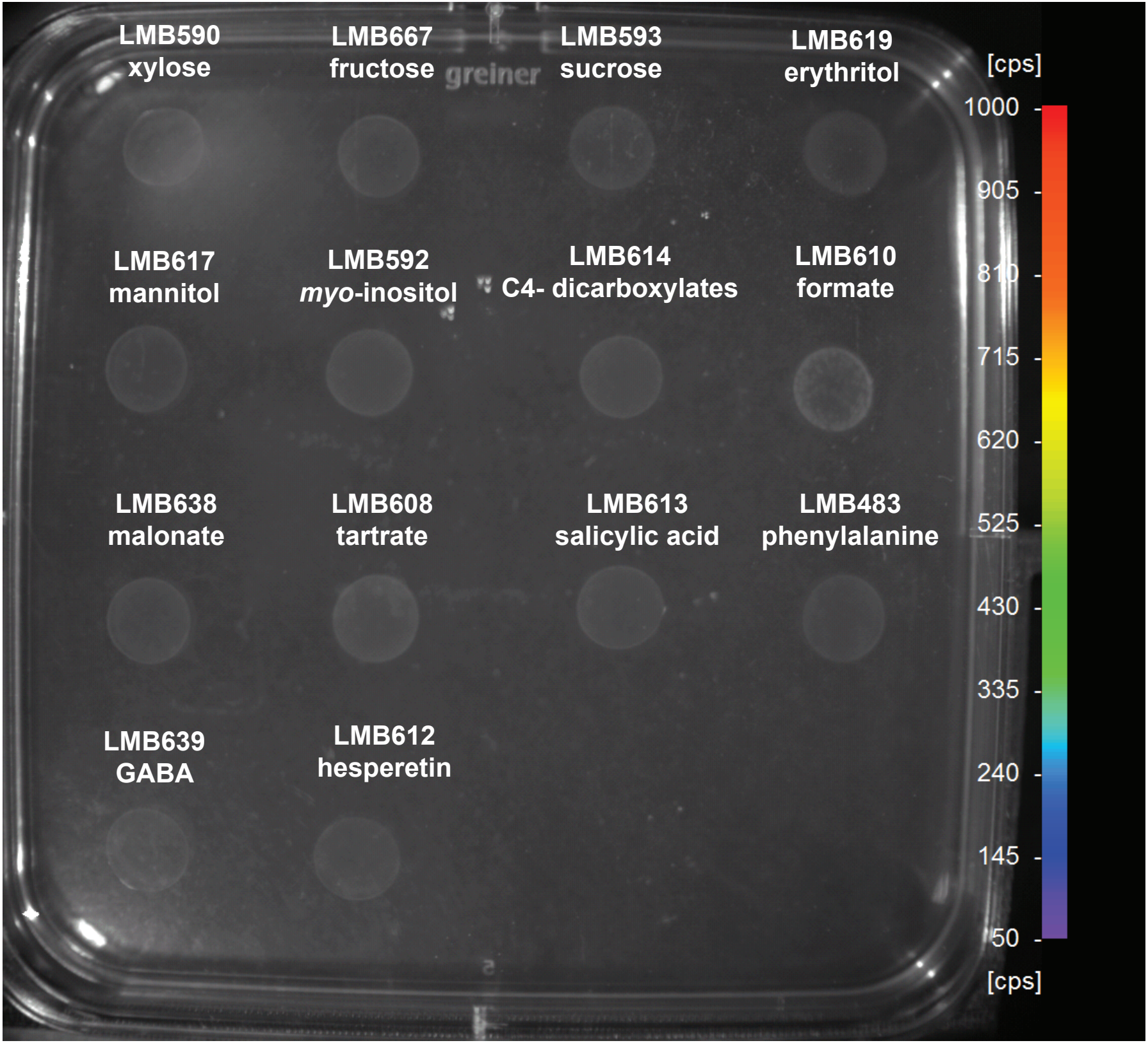
LMB590
xylose
LMB667
fructose
greiner
LMB593
sucrose
LMB619
erythritol
[cps]
1000
905
810
715
620
525
430
335
240
145
50
[cps]
LMB617
mannitol
LMB592
myo-inositol
LMB614
C4- dicarboxylates
LMB610
formate
LMB638
malonate
LMB608
tartrate
LMB613
salicylic acid
LMB483
phenylalanine
LMB639
GABA
LMB612
hesperetin

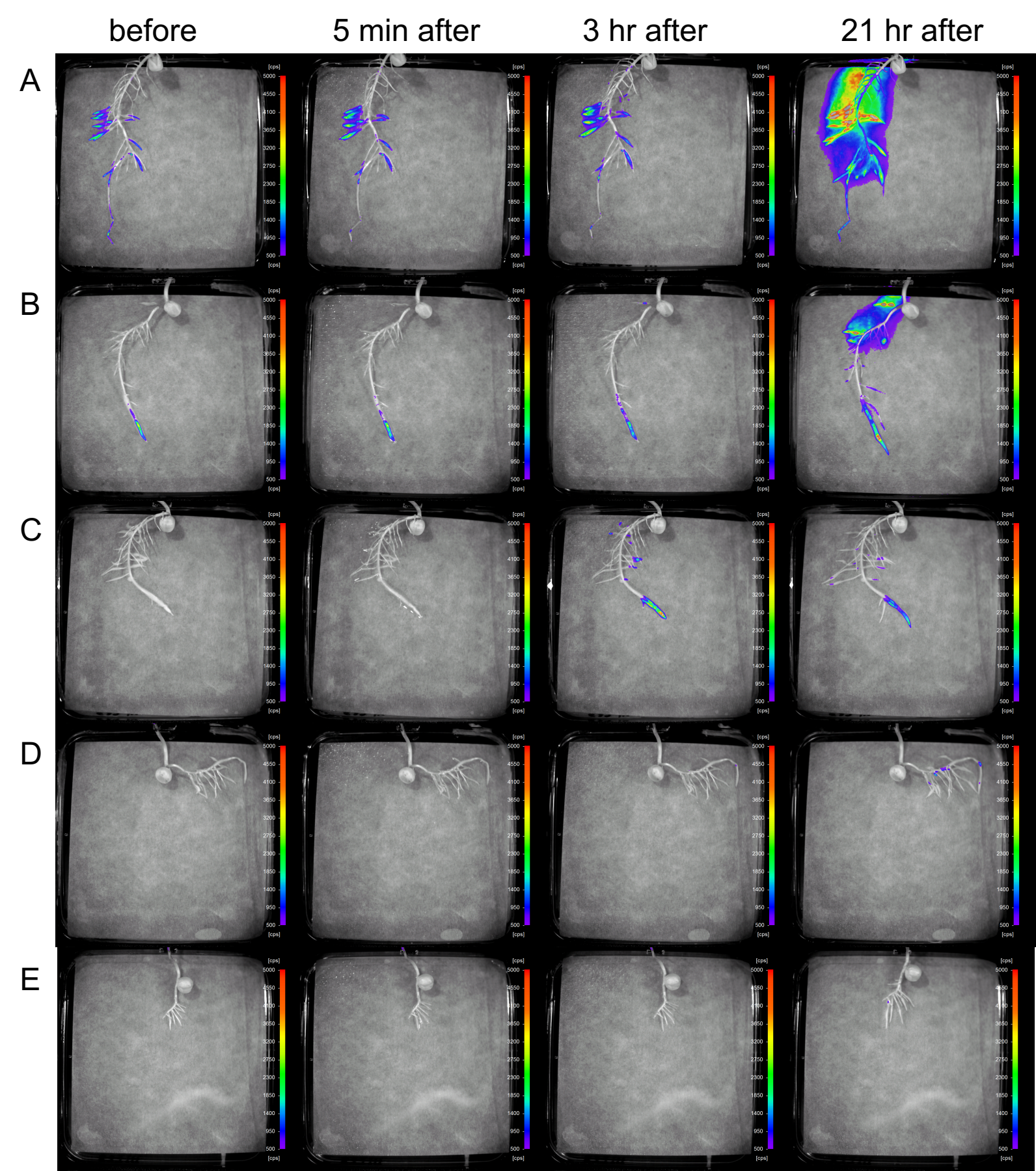
before
5 min after
3 hr after
21 hr after
A
B
C
D
E
[cps]
5000
4550
4100
3650
3200
2750
2300
1850
1400
950
500

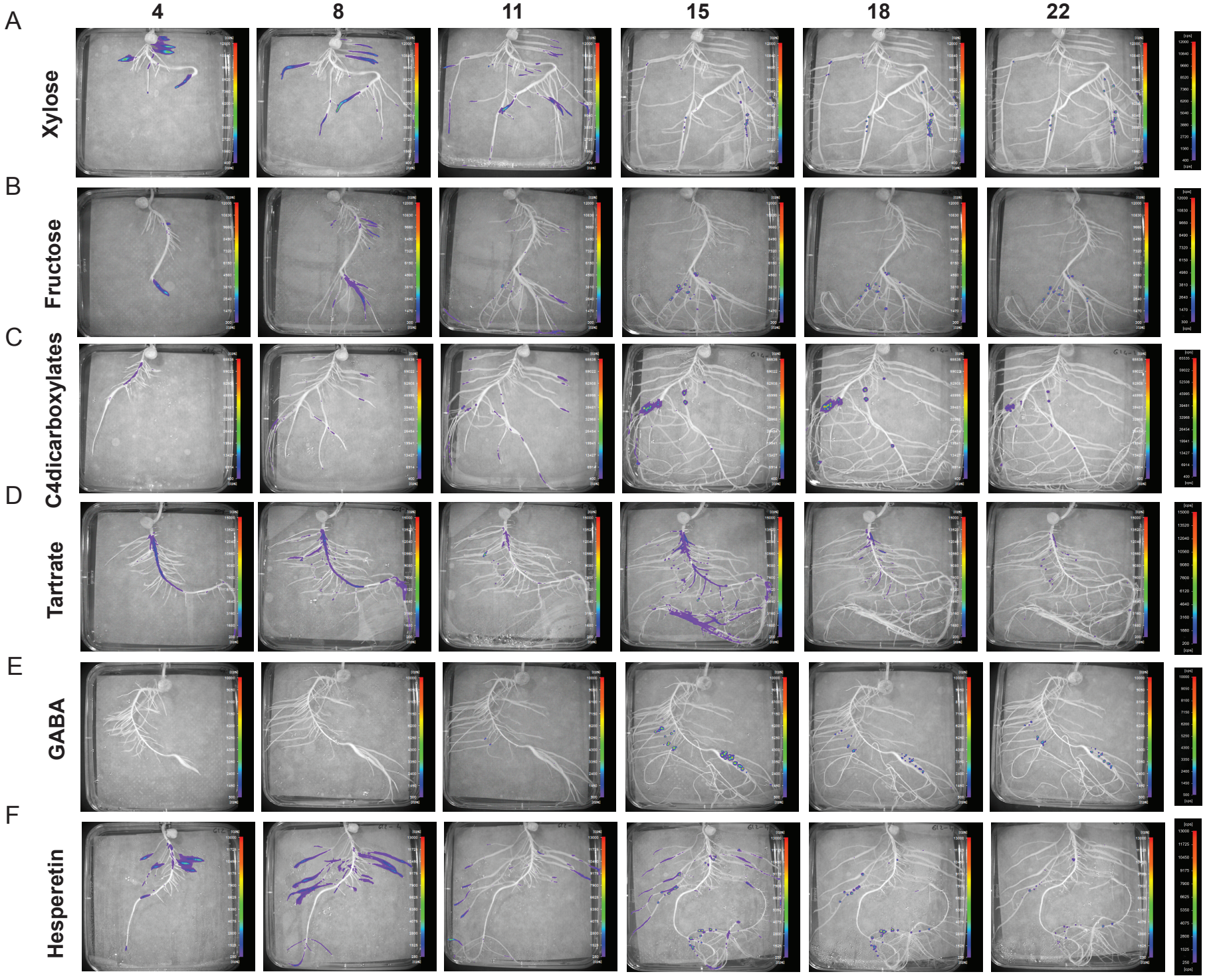
A
B
C
D
E
F
4
8
11
15
18
22
Xylose
Fructose
C4dicarboxylates
Tartrate
GABA
Hesperetin
Time [dpi]

Rlv3841

Rlv3841*nodC128*::Tn*5*

Rlv3841

Rlv3841*nodC128*::Tn*5*

A

B

C

D

Erythritiol

Mannitol

Formate

Salicylic acid

4 8 11 15 18 22

E

F

G

H

Mean intensity per pxl

0 5 10 15 20 25 30 35

0 5 10 15 20 25 30 35 40

4 8 11 15 18 22

Time [dpi]

I

J

K

L

[cps]

1000 910 820 730 640 550 460 370 280 190 100

700 635 570 505 440 375 310 245 180 115 50

2000 1810 1620 1430 1240 1050 860 670 480 290 100

150 138 126 114 102 90 78 66 54 42 30

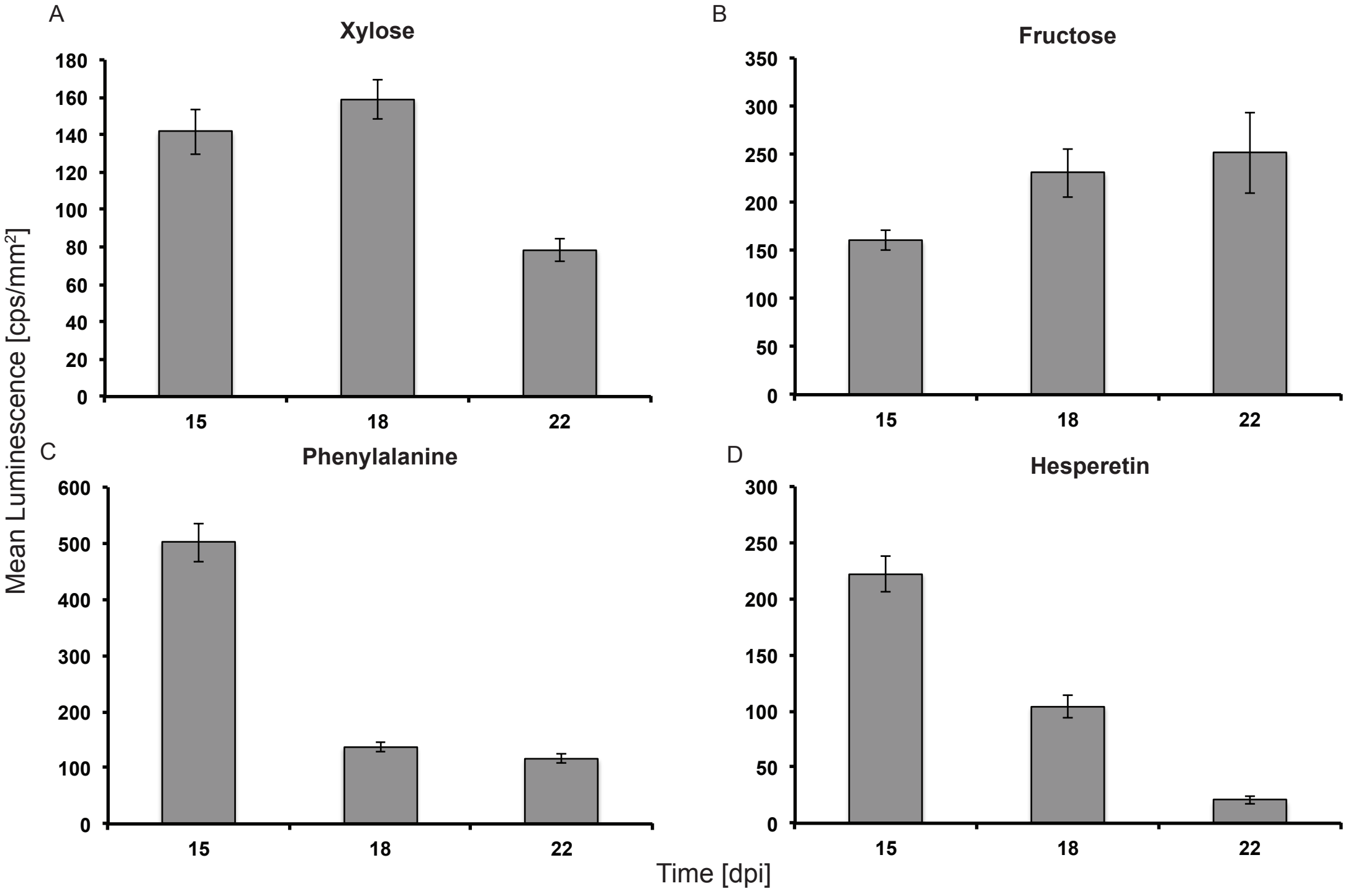
A
Xylose
180
160
140
120
100
80
60
40
20
0
15
18
22
B
Fructose
350
300
250
200
150
100
50
0
15
18
22
C
Phenylalanine
600
500
400
300
200
100
0
15
18
22
D
Hesperetin
300
250
200
150
100
50
0
15
18
22
Mean Luminescence [cps/mm²]
Time [dpi]

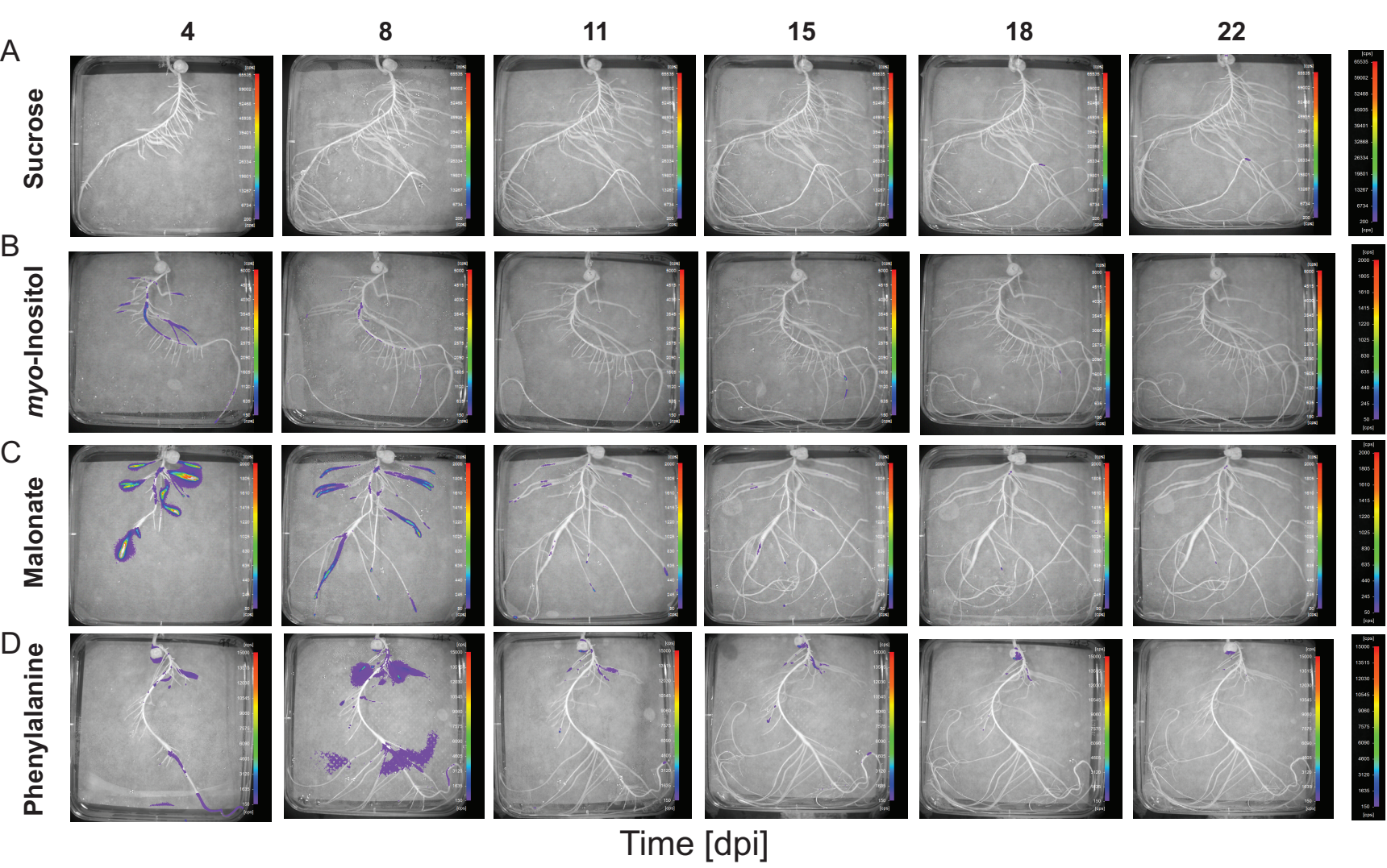
4
8
11
15
18
22
A
Sucrose
B
myo-Inositol
C
Malonate
D
Phenylalanine
Time [dpi]

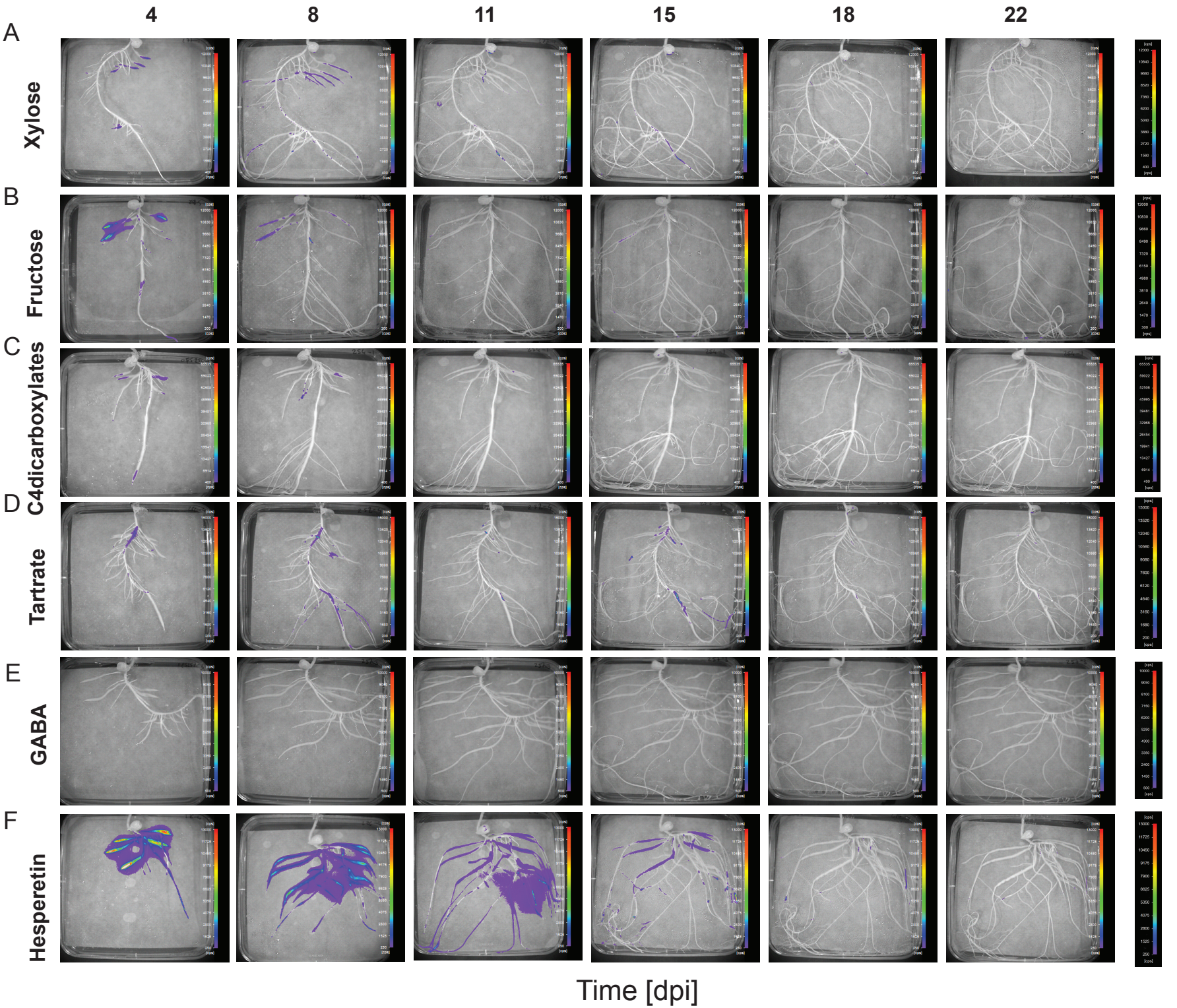
4
8
11
15
18
22
A
Xylose
B
Fructose
C
C4dicarboxylates
D
Tartrate
E
GABA
F
Hesperetin
Time [dpi]

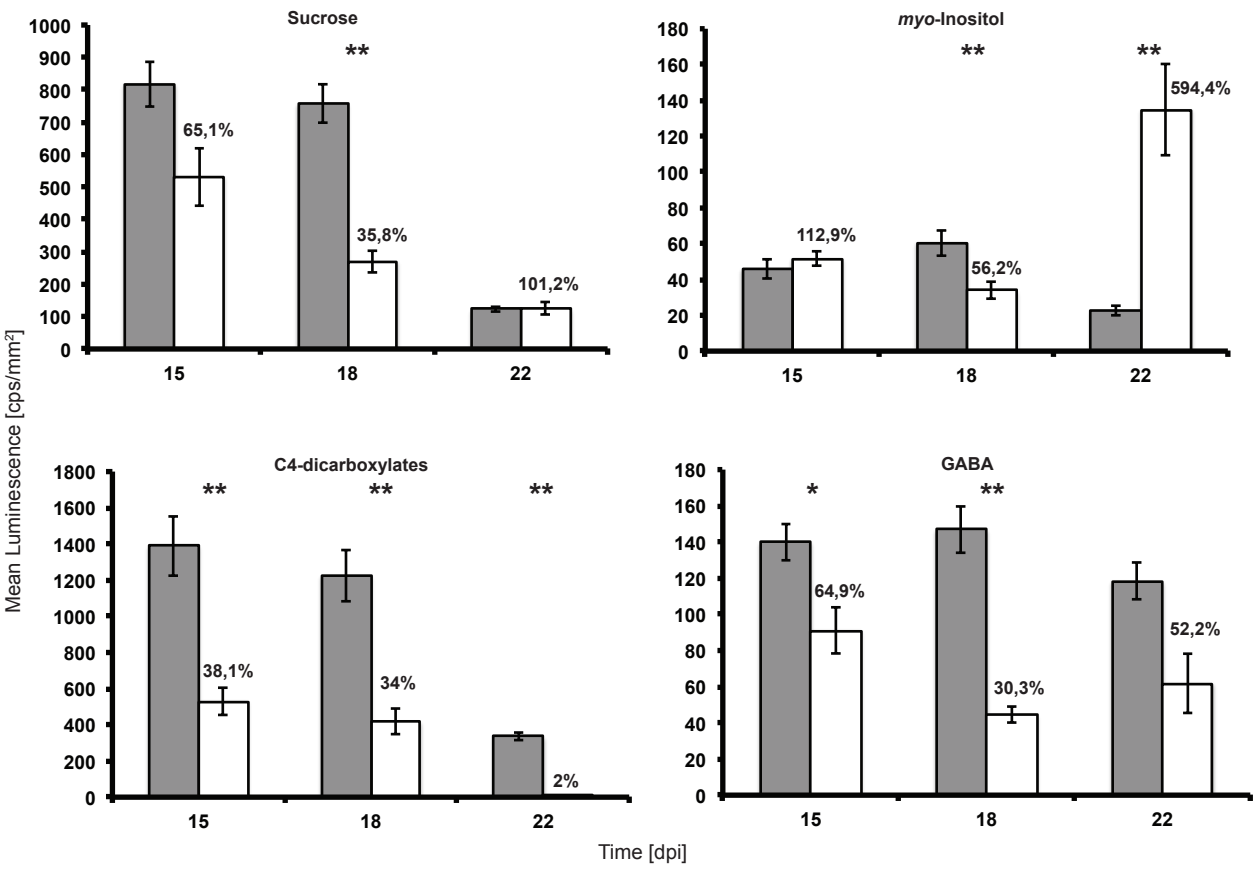
Sucrose
**
**
65,1%
35,8%
101,2%
1000
900
800
700
600
500
400
300
200
100
0
15
18
22
myo-Inositol
**
**
112,9%
56,2%
594,4%
180
160
140
120
100
80
60
40
20
0
15
18
22
C4-dicarboxylates
**
**
**
38,1%
34%
2%
1800
1600
1400
1200
1000
800
600
400
200
0
15
18
22
GABA
*
**
64,9%
30,3%
52,2%
180
160
140
120
100
80
60
40
20
0
15
18
22
Mean Luminescence [cps/mm²]
Time [dpi]

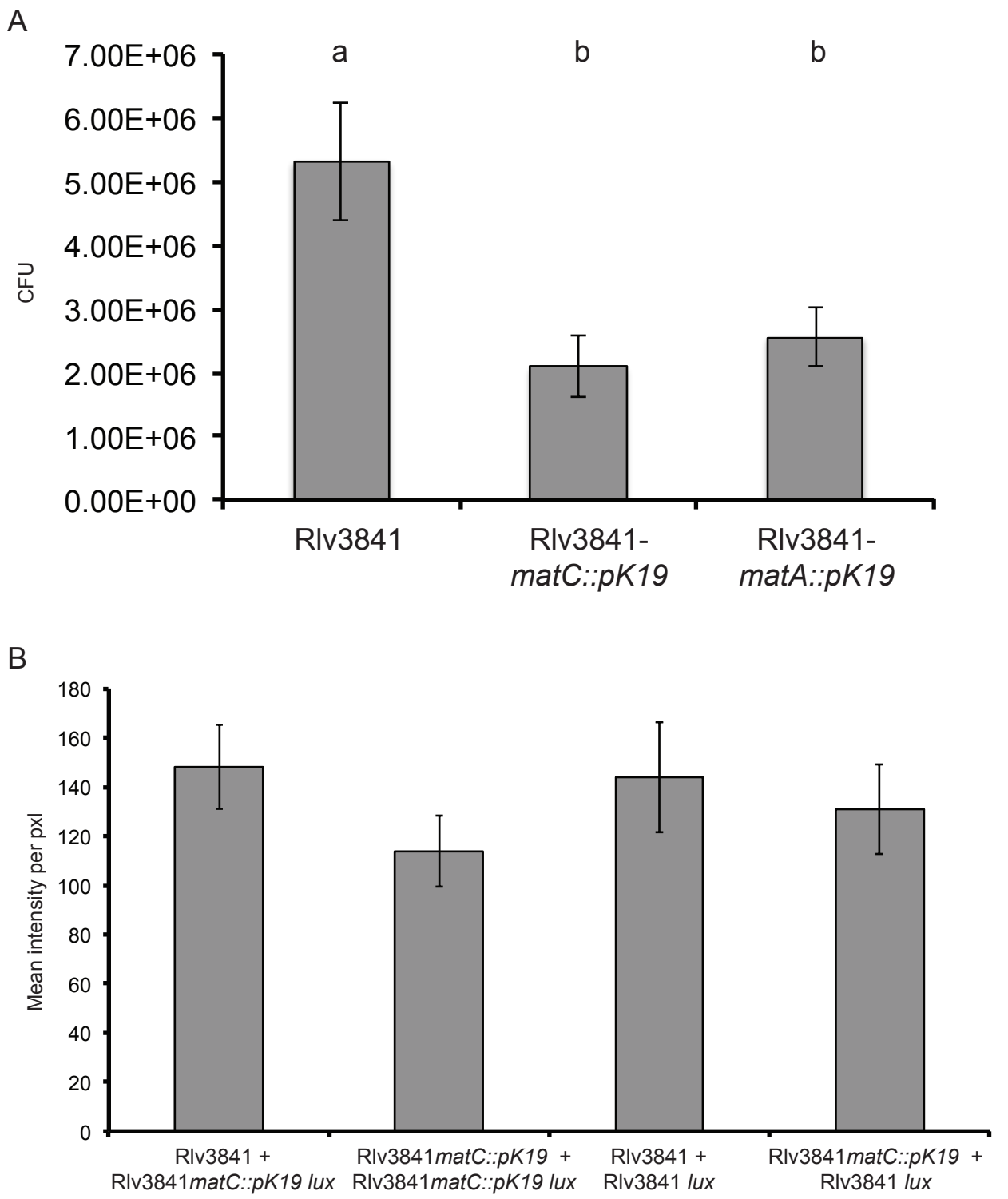
A
7.00E+06
6.00E+06
5.00E+06
4.00E+06
3.00E+06
2.00E+06
1.00E+06
0.00E+00
CFU
a
b
b
Rlv3841
Rlv3841-
matC::pK19
Rlv3841-
matA::pK19
B
180
160
140
120
100
80
60
40
20
0
Mean intensity per pxl
Rlv3841 +
Rlv3841matC::pK19 lux
Rlv3841matC::pK19 +
Rlv3841matC::pK19 lux
Rlv3841 +
Rlv3841 lux
Rlv3841matC::pK19 +
Rlv3841 lux